Available online at www.sciencedirect.com
ScienceDirect
Physics Reports 431 (2006) 261–302
PHYSICS REPORTS
www.elsevier.com/locate/physrep

Review on the symmetry-related properties of carbon nanotubes

Eduardo B. Barros[a,f], Ado Jorio[b], Georgii G. Samsonidze[f], Rodrigo B. Capaz[c,d], Antônio G. Souza Filho[a], Josué Mendes Filho[a], Gene Dresselhaus[e], Mildred S. Dresselhaus[f,*]

[a] *Departamento de Física, Universidade Federal do Ceará, Fortaleza, Ceará, CEP 60455-760, Brazil*
[b] *Departamento de Física, Universidade Federal de Minas Gerais, Belo Horizonte, MG, 30123-970 Brazil*
[c] *Instituto de Física, Universidade Federal do Rio de Janeiro, Caixa Postal 68528, Rio de Janeiro, RJ 21941-972, Brazil*
[d] *Divisão de Metrologia de Materiais, Instituto Nacional de Metrologia, Normalização e Qualidade Industrial - Inmetro, R. Nossa Senhora das Graças 50, Xerém, Duque de Caxias, RJ 25245-020, Brazil*
[e] *Francis Bitter Magnet Lab, Massachusetts Institute of Technology, Cambridge, MA 02139-4307, USA*
[f] *Departament of Electrical Engineering and Computer Science, Massachusetts Institute of Technology, Cambridge, MA 02139-4307, USA*

Accepted 24 May 2006
Available online 14 August 2006
editor: D.L. Mills

Abstract

In this work we review the basic properties of carbon nanotubes from the standpoint of group theory. The zone folding scheme is reviewed in the light of the helical symmetry of the nanotube. The group theory for chiral and achiral nanotubes is reviewed, and the representations of the factor group of the wavevector k are obtained. The similarities and differences between the formalism of the group of the wavevector and that of line groups are addressed with respect to the irreducible representations and quantum numbers associated with linear and angular momenta. Finally, we extend the results of group theory to illuminate the electronic and vibrational properties of carbon nanotubes. Selection rules for the optical absorption and double resonance Raman scattering are discussed for the case where the electron–electron interaction is negligible (metallic nanotubes) and for the case where exciton binding energies are strong and cannot be neglected.

PACS: 61.46.Fg; 61.50.Ah; 78.67.Ch

Contents

1. Introduction . . . 262
2. Carbon nanotube structure . . . 263
   2.1. Nanotube geometry and the (n, m) indices . . . 263
   2.2. Lattice vectors in real space . . . 264
   2.3. Lattice vectors in reciprocal space . . . 265
   2.4. Compound operations and tube helicity . . . 265
      2.4.1. Helical–helical construction . . . 266
      2.4.2. Linear–helical construction . . . 267

* Corresponding author.
E-mail addresses: ebarros@fisica.ufc.br (E.B. Barros), millie@mgm.mit.edu (M.S. Dresselhaus).

0370-1573/$ - see front matter © 2006 Published by Elsevier B.V.
doi:10.1016/j.physrep.2006.05.007

2.4.3. Helical–angular construction . . . 269
2.4.4. Linear–angular construction . . . 271
3. Group theory for carbon nanotubes . . . 271
3.1. Symmetries for chiral carbon nanotubes . . . 272
3.1.1. Group of the wave vector at the Γ point ($k = 0$) . . . 273
3.1.2. Group of the wave vector at a general point ($0 < k < \pi/T$) . . . 274
3.2. Group theory for achiral carbon nanotubes . . . 275
3.3. Eigenvectors and the irreducible representations . . . 277
3.4. Quantum numbers and crystal momentum . . . 278
4. Line groups vs. group of the wavevector . . . 279
4.1. Line group of chiral carbon nanotubes . . . 280
4.2. Eigenvectors and the irreducible representations . . . 282
4.3. Quantum numbers and crystal momentum . . . 283
5. Electronic band structure . . . 283
5.1. Symmetry of electronic states from the line group approach . . . 286
6. Phonons in carbon nanotubes . . . 287
7. Selection rules for optical phenomena . . . 289
7.1. Selection rules for optical absorption from space group theory . . . 289
7.2. Selection rules for Raman and infrared spectroscopy from group theory . . . 289
7.3. Selection rules for double resonance Raman processes . . . 290
7.4. Selection rules from zone folding . . . 291
8. Excitons in carbon nanotubes . . . 293
8.1. The exciton symmetries . . . 293
8.1.1. Chiral nanotubes . . . 294
8.1.2. Zigzag nanotubes . . . 297
8.1.3. Armchair nanotubes . . . 297
8.2. Selection rules for optical absorption . . . 298
8.3. Selection rules for Raman scattering processes . . . 299
9. Summary and conclusions . . . 300
Acknowledgments . . . 300
References . . . 301

1. Introduction

The symmetry properties of carbon nanotubes have been a subject of intense discussion from the very beginning of the study of carbon nanotubes [1–3]. However, the earlier description was not complete, and much work was required to achieve a full description of the nanotube symmetry-related properties [4–7]. Also, Saito et al. used the zone-folding scheme to obtain, as a first approximation, the electronic and vibrational properties of carbon nanotubes [3]. Within this scheme, the properties of the nanotube are obtained directly from that of a graphene sheet by imposing the confinement of the wavefunctions in the circumferential direction, neglecting curvature effects.

The symmetry properties of periodic lattices are usually described in terms of the group of the wavevector [8]. However, since nanotubes can be viewed as quasi-1D systems, the line group approach is suited to describe nanotube properties as well. The line group approach to nanotubes was described by Damnjanović et al. [4]. Much confusion can arise from the use of these two different formalisms to describe the symmetry of the nanotubes. It is thus imperative to develop a full description of the carbon nanotube symmetry from the standpoint of the factor group of the wavevector and then to make a direct comparison with the symmetry properties of carbon nanotubes obtained using the formalism of line groups.

To obtain a detailed group theoretical analysis of carbon nanotubes we begin in Section 2 by giving a summary of the structural properties of carbon nanotubes in real and reciprocal space. In Section 3, we describe the symmetry operations of chiral and achiral nanotubes and obtain the representations for each of the symmetry operations in view of factor group of the translational sub-group of the wavevector, as is common in general space group theory. In this section, the irreducible representations and the quantum numbers which are used to label them are compared to the symmetry properties and selection rules obtained from “zone-folding” of the reciprocal space of 2D graphite, as described in Section 2. In Section 4, the review continues with a comparison between the symmetry properties of nanotubes obtained using the formalism of the group of the wavevector and the formalism of line groups. The focus

of this section is on chiral nanotubes. For a better comprehension of the symmetry-related properties of nanotubes, in Section 5 we discuss the symmetry of the electronic eigenstates using both the group of the wavevector and the approach of line groups. Furthermore, the symmetry-related properties of phonons in carbon nanotubes are discussed in Section 6, from the standpoint of the group of the wavevector developed in Section 3, and within the "zone-folding" scheme. These sections are followed by a description of the selection rules for optical phenomena in Section 7, neglecting the exciton interaction. The excitonic interaction is then described in Section 8 within a simple model that gives insight into the symmetry properties of the excitonic states and how they affect the selection rules for optical phenomena. The paper is concluded in Section 9 with a summary of the main results obtained here and the conclusions that can be drawn from this review about the symmetry of carbon nanotubes.

2. Carbon nanotube structure

Carbon nanotubes can be viewed as a graphene sheet (a single layer from a 3D graphite crystal) rolled up into a cylinder, one atomic layer in thickness. The nanotube physical properties depend on how the graphene sheet is rolled up, and from a symmetry point of view, two types of nanotubes can be formed, namely the achiral armchair or zigzag tubes, as shown in Figs. 1(a) and (b), respectively, and the chiral tubes, as shown in Fig. 1(c).

Because of the small diameter of a carbon nanotube ($\sim$ 1 nm) and the large length-to-diameter ratio ($> 10^4$), carbon nanotubes are an important system for studying one-dimensional physics, both theoretically and experimentally. Therefore, in discussing the symmetry of carbon nanotubes, it is assumed that the nanotube length is much larger than its diameter, so that the nanotube ends (see Fig. 1) can be neglected when discussing the electronic and lattice properties of the nanotubes. Thus from a symmetry standpoint, a carbon nanotube is a one-dimensional crystal with a translation vector $\vec{T}$ along the cylinder axis and a small number of carbon hexagons associated with the circumferential direction.

2.1. Nanotube geometry and the (n, m) indices

A single wall carbon nanotube (SWNT) is constructed starting from a strip of a graphene layer (see Fig. 2) by rolling it up into a seamless cylinder. The nanotube structure is uniquely determined by the chiral vector $\vec{C}_h$ which spans the

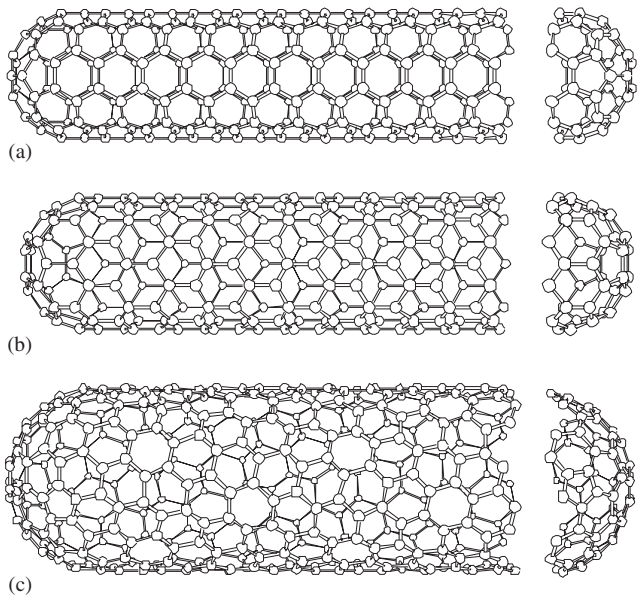

Fig. 1. Schematic theoretical model for examples of the three different types of single-wall carbon nanotubes: (a) the "armchair" nanotube; (b) the "zigzag" nanotube; and (c) the "chiral" nanotube. The actual nanotubes shown in the figure correspond to (n, m) values of: (a) (5, 5), (b) (9, 0), and (c) (10, 5)—see text [3].

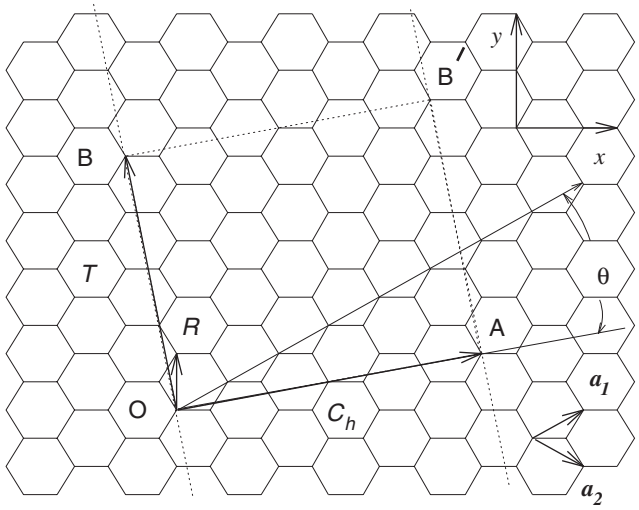

Fig. 2. An unrolled nanotube unit cell projected on the graphene layer. When the nanotube is rolled up, the chiral vector $\vec{C}_h$ turns into the circumference of the cylinder, and the translation vector $\vec{T}$ is aligned along the cylinder axis. $\vec{R}$ is the symmetry vector (Section 2.4) and θ is the chiral angle. The unit vectors $(\vec{a}_1, \vec{a}_2)$ of the graphene layer are indicated in the figure along with the inequivalent A and B sites within the unit cell of the graphene layer given by a hexagon. The unit cell of the nanaotube is defined by the rectangle delimited by the vectors $\vec{C}_h$ and $\vec{T}$ [3].

circumference of the cylinder when the graphene layer is rolled up into a tube. The chiral vector can be written in the form $\vec{C}_h = n\vec{a}_1 + m\vec{a}_2$, where the vectors $\vec{a}_1$ and $\vec{a}_2$ bound the unit cell of the graphene layer, which contains the two distinct carbon atom sites A and B. The values of n and m are arbitrary integer numbers which uniquely characterize the nanotube structure. In the shortened (n, m) form, the chiral vector is written as a pair of integers, and the same notation is widely used to characterize the geometry of each distinct (n, m) nanotube [3].

The nanotube can also be characterized by its diameter d_t and chiral angle θ, which determine the length $C_\mathrm{h}=|\vec{C}_h|=\pi d_t$ of the chiral vector and its orientation on the graphene layer (see Fig. 2). Both d_t and θ are expressed in terms of the indices n and m by the relations $d_t = a\sqrt{n^2 + nm + m^2}/\pi$ and $\tan\theta = \sqrt{3}m/(2n + m)$, as one can derive from Fig. 2, where $a = \sqrt{3}a_{\mathrm{C-C}} = 0.246$ nm is the lattice constant for the graphene layer and $a_{\mathrm{C-C}} = 0.142$ nm is the nearest neighbor C–C distance. As an example, the chiral vector $\vec{C}_h$ shown in Fig. 2 is given by $\vec{C}_h = 4\vec{a}_1 + 2\vec{a}_2$, and thus the corresponding nanotube can be identified by the pair of integers $(n, m) = (4, 2)$. Due to the six-fold symmetry of the graphene layer, all non-equivalent nanotubes can be characterized by the (n, m) pairs of integers where $0 \leqslant m \leqslant n$. It is also possible to define nanotubes with opposite handedness, for which $0 \leqslant n \leqslant m$ [9]. The nanotubes are classified as chiral $(0 < m < n)$ and achiral ($m = 0$ or $m = n$), which in turn are known as zigzag ($m = 0$) and armchair ($m = n$) nanotubes (see Figs. 1 and 2). A (4, 2) nanotube is one of the smallest diameter nanotubes ever synthesized [10].

It should be mentioned here that, for small diameter nanotubes ($d_t < 1$ nm), the geometrical structure of the nanotube will be slightly different from that of a rolled up graphene layer. For a correct description of the nanotube properties, it is necessary to take the geometrical structure relaxation due to the curvature effect into account [11,12].

2.2. Lattice vectors in real space

To specify the symmetry properties of carbon nanotubes as 1D systems, it is necessary to define the lattice vector or translation vector $\vec{T}$ along the nanotube axis and normal to the chiral vector $\vec{C}_h$ defined in Fig. 2. The vectors $\vec{T}$ and $\vec{C}_h$ define the unit cell of the 1D nanotube. The translation vector $\vec{T}$, of a general chiral nanotube as a function of n and m, can be written as $\vec{T} = t_1\vec{a}_1 + t_2\vec{a}_2$, where $t_1 = (2m + n)/d_R$ and $t_2 = -(2n + m)/d_R$. The length of the translation vector is $T = \sqrt{3}C_\mathrm{h}/d_R$, where d is the greatest common divisor of (n, m) (denoted by $gcd(n, m)$), and d_R is the greatest common divisor of $2n + m$ and $2m + n$. Then d and d_R are related by [3]

$$d_R = \begin{cases} d & \text{if } n - m \text{ is not a multiple of } 3d, \\ 3d & \text{if } n - m \text{ is a multiple of } 3d. \end{cases} \tag{1}$$

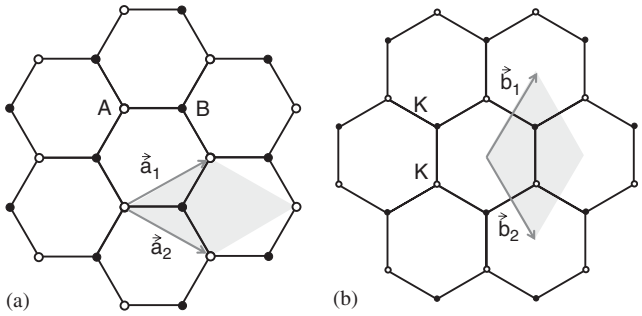

Fig. 3. (a) Real space lattice of a graphene layer. The rhombus represents the graphene unit cell with lattice vectors $\vec{a}_1$ and $\vec{a}_2$ delimiting it. Note that this area encloses a total of 2 atoms, one A atom and one B atom. (b) Reciprocal space lattice of the a graphene layer showing the unit vectors $\vec{b}_1$ and $\vec{b}_2$. Note also that the reciprocal space structure has two inequivalent points K and K'.

For the (4, 2) nanotube shown in Fig. 2, we have $d_R = d = 2$ and $(t_1, t_2) = (4, -5)$. For armchair and zigzag achiral tubes, $T = a$ and $\sqrt{3}a$, respectively. The unit cell of an unrolled nanotube on a graphene layer is a rectangle bounded by the vectors $\vec{C}_h$ and $\vec{T}$ (see the rectangle shown in Fig. 2 for the (4, 2) nanotube). The area of the nanotube unit cell can be easily calculated as a vector-product of these two vectors, $|\vec{C}_h \times \vec{T}| = \sqrt{3}a^2(n^2 + nm + m^2)/d_R$. Dividing this product by the area of the unit cell of a graphene layer $|\vec{a}_1 \times \vec{a}_2| = \sqrt{3}a^2/2$, one can get the number of hexagons in the unit cell of a nanotube,

$$N = \frac{2(n^2 + nm + m^2)}{d_R}. \tag{2}$$

For the (4, 2) nanotube we have $N = 28$, so that the unit cell of the (4, 2) nanotube (see the rectangle shown in Fig. 2) contains 28 hexagons, or $2 \times 28 = 56$ carbon atoms. For armchair (n, n) and zigzag $(n, 0)$ tubes, $N = 2n$.

2.3. Lattice vectors in reciprocal space

The graphene reciprocal lattice unit vectors $\vec{b}_1$ and $\vec{b}_2$ can be constructed from the real space lattice vectors $\vec{a}_1$ and $\vec{a}_2$ using the standard definition $\vec{a}_i \cdot \vec{b}_j = 2\pi\delta_{ij}$, where δ_{ij} is the Kroneker delta symbol. In Figs. 3(a) and (b) we show the real and reciprocal space lattice of a graphene sheet, correspondingly. Note the difference of 30° in the orientation of the hexagons in real space (Fig. 3(a)) with respect to those in reciprocal space (Fig. 3(b)).

In a similar fashion, the reciprocal space of a nanotube can be constructed, if we consider the nanotube as a 1D system with an internal structure that is composed of the $2N$ atoms in its unit cell and with a translational symmetry given by the translation vector $\vec{T}$. The reciprocal space of the nanotube can be constructed by finding a pair of reciprocal lattice vectors $\vec{K}_1$ and $\vec{K}_2$ which satisfy: $\vec{C}_h \cdot \vec{K}_1 = \vec{T} \cdot \vec{K}_2 = 2\pi$ and $\vec{C}_h \cdot \vec{K}_2 = \vec{T} \cdot \vec{K}_1 = 0$. Due to the spatial confinement of the nanotube in the circumferential direction, the vector $\vec{C}_h$ does not play the role of a translation vector, rather it acts as a generator of pure rotations. In this sense, the relation $\vec{C}_h \cdot \vec{K}_1 = 2\pi$ can only be satisfied for $\vec{K}_1$ being integer multiples of $2/d_t$, where d_t is the diameter of the nanotube. This approach was used by Saito et al. to obtain the properties of nanotubes from those of a graphene layer by means of "zone-folding" and "zone-unfolding" [3]. Although the "zone-folding" approach is easy to understand in its geometrical construction, the literature lacks a rigorous mathematical formalism to explain this approach. As we discuss in Section 2.4, the mathematical basis of the zone-folding scheme lies in the presence of the screw operations of the nanotubes, which allows for the nanotube to be represented in terms of a reduced unit cell composed of only 2 atoms, similar to a graphene layer unit cell. Thus, by using the screw translations, the properties of the nanotube can be directly related to those of a graphene layer.

2.4. Compound operations and tube helicity

All multiples of the translation vector $\vec{T}$ will be translational symmetry operations of the nanotube [13]. However, to be more general, it is necessary to consider that any lattice vector

$$\vec{t}_{p,q} = p\vec{a}_1 + q\vec{a}_2, \tag{3}$$

with p and q integers, of the unfolded graphene layer will also be a symmetry operation of the tube. In fact, the symmetry operation that arises from $\vec{t}_{p,q}$ will appear as a screw translation of the nanotube. Screw translations are combinations of a rotation by an angle ϕ (R_ϕ) and a translation $\vec{\tau}$ in the axial direction of the nanotube. The screw translation can be written as $\{R_\phi|\tau\}$, using a notation common for space group operations [3,8].

The translation vector $\vec{t}_{p,q}$ can also be written in terms of components of the nanotube lattice vectors, $\vec{T}$ and $\vec{C}_h$, as

$$\vec{t}_{p,q} = \vec{t}_{u,v} = (u/N)\vec{C}_h + (v/N)\vec{T}, \tag{4}$$

where u and v are given by

$$u = \frac{(2n+m)p + (2m+n)q}{d_R} \tag{5}$$

and

$$v = mp - nq. \tag{6}$$

Both u and v are integer numbers which can assume either negative or positive values.

The screw translation of the nanotube which is associated with the graphene lattice vector $\vec{t}_{u,v}$ can then be written as

$$\vec{t}_{u,v} = \{C_N^u|vT/N\}, \tag{7}$$

where C_N^u is a rotation of $u(2\pi/N)$ around the nanotube axis, and $\{E|vT/N\}$ is a translation of vT/N along the nanotube axis, with T being the magnitude of the primitive translation vector $\vec{T}$. It is clear that if a screw vector $\{C_N^u|vT/N\}$ is a symmetry operation of the nanotube, then the vectors $\{C_N^u|vT/N\}^s$, for any integer value of s, are also symmetry operations of the nanotube. The number of hexagons in the unit-cell N assumes the role of the "order" of the screw axis, since the symmetry operation $\{C_N^u|vT/N\}^N = \{E|vT\}$, where E is the identity operator, and $v\vec{T}$ is a pure translation of the nanotube.

The nanotube structure can be obtained from a small number of atoms (between 2 and $2N$) by using any choice of two non-colinear screw vectors $\{C_N^{u_1}|v_1T/N\}$ and $\{C_N^{u_2}|v_2T/N\}$. Two vectors are colinear if there exists a pair of integers s and l different from 1, for which $lu_1 = su_2 + \lambda N$, and $lv_1 = sv_2 + \gamma T$, where λ and γ are two arbitrary integers. The area of the nanotube cylindrical surface delimited by these two non-colinear vectors can be regarded as a reduced unit cell. Note that the number of atoms in this reduced unit cell is given by the ratio between the area delimited by these vectors ($|\vec{t}_{u_1,v_1} \times \vec{t}_{u_2,v_2}|$) and the area of the unit cell of a graphene sheet ($|\vec{a}_1 \times \vec{a}_2|$) multiplied by 2, for A and B atoms in the graphene unit cell. Thus the number of atoms in the reduced unit cell defined by t_{u_1,v_1} and t_{u_2,v_2} is given by

$$2\frac{|\vec{t}_{u_1,v_1} \times \vec{t}_{u_2,v_2}|}{|\vec{a}_1 \times \vec{a}_2|} = 2\frac{|v_2u_1 - u_2v_1|}{N}. \tag{8}$$

It is important to point out that, in this case, the nanotube ceases to be described as a quasi-1D system, but as a system with two quasi-translational dimensions, which are generated by the two screw vectors.

There are many combinations of screw vectors that can be used to construct the nanotube. These combinations can be divided into four categories: helical–helical, linear–helical, helical–angular and linear–angular, as described below.

2.4.1. Helical–helical construction

The helical–helical construction is pertinent when two general non-colinear screw axes are used to construct the nanotube, denoted by the non-colinear vectors $\vec{t}_{u_1,v_1}$ and $\vec{t}_{u_2,v_2}$, after Eq. (4). With a convenient choice of screw vectors, it is possible to obtain the nanotube structure from a motif that has only two atoms, as in the unit-cell of graphene. The most obvious choice of screw vectors that will define a reduced unit cell with only two atoms is the screw vectors corresponding to the lattice vectors $\vec{a}_1$ and $\vec{a}_2$ of the graphene unit cell. It can be seen from Eqs. (5) and (6) that these screw vectors will be obtained by choosing $u_1 = (2n+m)/d_R$, $v_1 = m$, $u_2 = (2m+n)/d_R$, $v_2 = -n$. In the case of the (4, 2) nanotube, these screw vectors can be written as $\{C_{28}^5|T/14\}$ and $\{C_{28}^4|-T/7\}$. Fig. 4(a) shows the shape of the 2-atom reduced unit cell of a (4, 2) nanotube. The shape of this reduced unit cell can be understood as the projection of the unit cell of the graphene layer onto the cylindrical surface of the nanotube.

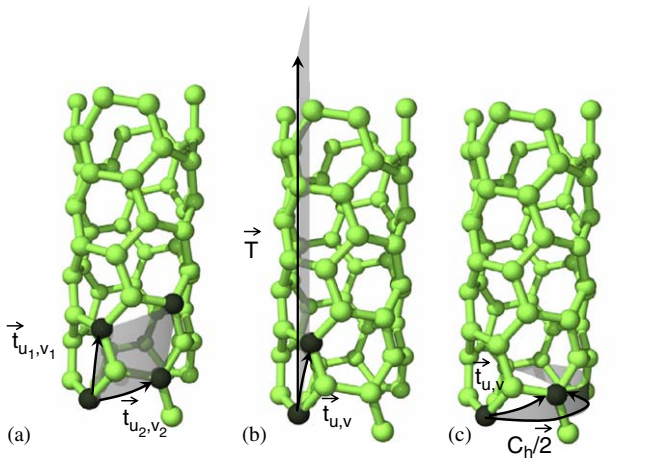

Fig. 4. 2-atom reduced unit cell for the (a) helical–helical construction, (b) linear–helical construction and (c) helical–angular construction for a (4, 2) nanotube.

The 2D reciprocal lattice vectors of the nanotube $\vec{\kappa}_1$ and $\vec{\kappa}_2$, which follow the relation $\vec{t}_{u_1,v_1} \cdot \vec{\kappa}_1 = \vec{t}_{u_2,v_2} \cdot \vec{\kappa}_2 = 2\pi$ and $\vec{t}_{u_1,v_1} \cdot \vec{\kappa}_2 = \vec{t}_{u_2,v_2} \cdot \vec{\kappa}_1 = 0$ can be written in terms of the reciprocal lattice vectors $\vec{K}_1$ and $\vec{K}_2$ as

$$\vec{\kappa}_1 = \frac{Nv_2}{v_2u_1 - u_2v_1}\vec{K}_1 - \frac{Nu_2}{v_2u_1 - u_2v_1}\vec{K}_2 \tag{9}$$

and

$$\vec{\kappa}_2 = -\frac{Nv_1}{v_2u_1 - u_2v_1}\vec{K}_1 + \frac{Nu_1}{v_2u_1 - u_2v_1}\vec{K}_2. \tag{10}$$

From Eq. (8), we see that the number of atoms in the reduced unit cell is proportional to $v_2u_1 - u_2v_1$ and thus this number will not be zero for any choice of screw vectors that yield the nanotube structure.

In the case where (u_1, v_1) and (u_2, v_2) are chosen so that the number of atoms in the reduced unit cell is 2, the reciprocal lattice vectors of the nanotube become the lattice vectors $\vec{b}_1$ and $\vec{b}_2$ of the graphene reciprocal space. The highest order symmetry operation of the nanotube, which maintains this unit cell invariant is a rotation of π around an axis perpendicular to the nanotube axis and which goes through the center of a hexagon, or between the two inequivalent atoms. For achiral nanotubes, there are other symmetry operations such as mirror planes and inversion centers, but they are all of order 2. With the exception of the case of zigzag tubes, neither of the graphene reciprocal space unit vectors $\vec{b}_1$ and $\vec{b}_2$ are aligned with the translation vector $\vec{T}$ nor with the pure rotations of the nanotube $\vec{C}_h$. Therefore, in the case of a general chiral nanotube, the helical–helical construction will not be the best choice to describe the nanotube properties.

2.4.2. Linear–helical construction

The linear–helical construction is obtained when one of the screw vectors is chosen to be the translational vector $\vec{T}$ while the other screw vector is a general one, which will be written as $\{C_N^u|vT/N\}$ in the screw axis notation. The translational vector $\vec{T}$ plays the role of the generator of translations, while the screw vector $\{C_N^u|vT/N\}$ plays the role of a quasi-rotational symmetry. Substituting $\vec{T}$ as one of the screw vectors in Eq. (8), the number of atoms in the reduced unit cell of the nanotube is found to be $2u$. Therefore, by choosing a screw vector with $u = 1$, it is also possible to construct the nanotube from only two atoms. Substituting $u = 1$ in Eqs. (5) and (6) gives the relation for v:

$$v = \frac{md_R}{(2n+m)} - \frac{N}{(2n+m)}q, \tag{11}$$

where q has to be conveniently chosen so that v is an integer and is within the first unit-cell of the nanotube. Due to the symmetry of the nanotube upon a rotation perpendicular to the nanotube axis, for any given (n, m) nanotube there are two equivalent vectors which follow Eq. (11) within the first unit-cell, one for $q > 0$ and another for $q < 0$. These

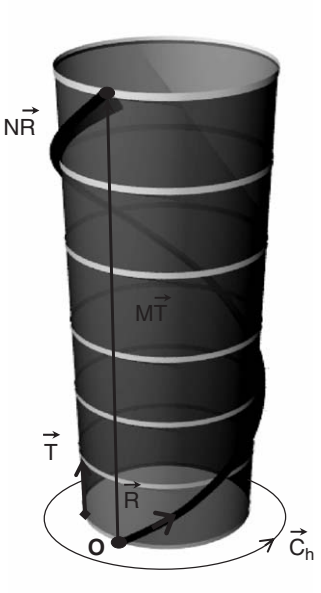

Fig. 5. The vector $\vec{R} = \{C_N^u | vT/N\}$, with $u = 1$ and $v = M$, is shown on the cylindrical surface, starting from O. The effect of applying $\vec{R}$ N times ($N\vec{R} = \{C_N^u | vT/N\}^N$) is depicted as an helicoidal path. After rotating by 2π around the tube, the vector $N\vec{R}$ reaches a lattice point equivalent to point O, but separated from O by $M\vec{T}$. In the figure we show the case $\vec{C}_h = (4, 2)$ where $v = M = 6$.

vectors are related by $|v^+| = N - |v^-|$ and, to avoid ambiguity, the smallest value of v should always be used. By choosing this vector, we reproduce the symmetry vector $\vec{R}$ defined by Saito et al. [3] for which the value v was denoted by M. Note that M can be regarded as the number of unit cells spanned by the screw vector $\vec{R}$ when it is applied N times, as shown in Fig. 5. Another characteristic of $\vec{R}$ is that the nanotube is rotated by exactly 2π when the screw vector $\vec{R}$ is applied N times. The 2-atom reduced unit cell, in this case, has a rhombic shape projected on the cylindrical surface with one of the sides coinciding with the translational vector $\vec{T}$ and other aligned with the screw vector $\vec{R}$. The highest symmetry operation of this unit cell is also the π rotation perpendicular to the nanotube axis. In Fig. 4(b) we show the 2-atom reduced unit-cell of the (4, 2) nanotube for the linear–helical construction, where the screw vector $\vec{R}$ has components $u = 1$ and $v = M = 6$. To better illustrate the action of the screw vector $\vec{R}$, we show in Fig. 6(a) a diagram of the (4, 2) nanotube. The dark atoms in the bottom represent a 2-atom motif. We also show another set of atoms in dark which is equivalent to this motif due to a rotation of $2\pi/d$, with $d = 2$, around the nanotube axis. The dark-grey helix of atoms is composed of the atoms in the nanotube unit cell which can be obtained by consecutive applications of the screw vector $\vec{R}$ to the atoms in the motif, while the light-grey atoms are obtained by successive operations of the screw vector $\vec{R}$ followed by a pure translation which brings the motif back to the original unit cell. For better visualization, a 2D diagram of the unfolded unit cell of the (4, 2) nanotube is shown in Fig. 6(b). In this diagram, the 2-atom motif is depicted as an ellipse and each helix in the nanotube is depicted as a dashed line. Note that the translation vector $\vec{T}$ connects one motif in this unit cell (full dark ellipse) to an equivalent motif in the next unit cell (open ellipse).

By substituting the two unit vectors of the linear–helical construction (the translation vector $\vec{T}$ and a general screw vector $\vec{t}_{u,v}$) into Eqs. (9) and (10), we find the reciprocal lattice vectors to be

$$\vec{\kappa}_1 = (N/u)\vec{K}_1, \tag{12}$$

and

$$\vec{\kappa}_2 = \vec{K}_2 - (v/u)\vec{K}_1. \tag{13}$$

The Brillouin zone of this reciprocal space is delimited by the vectors $\vec{\kappa}_1$ and $\vec{\kappa}_2$. However, since $\vec{\kappa}_1$ is perpendicular to the cutting lines, it is convenient to define the Brillouin zone as a rectangle composed of N/u cutting lines of length $2\pi/T$ which can be translated by the vectors $\vec{\kappa}_1$ and $\vec{\kappa}_2$ to cover all of reciprocal space. It is important to notice that

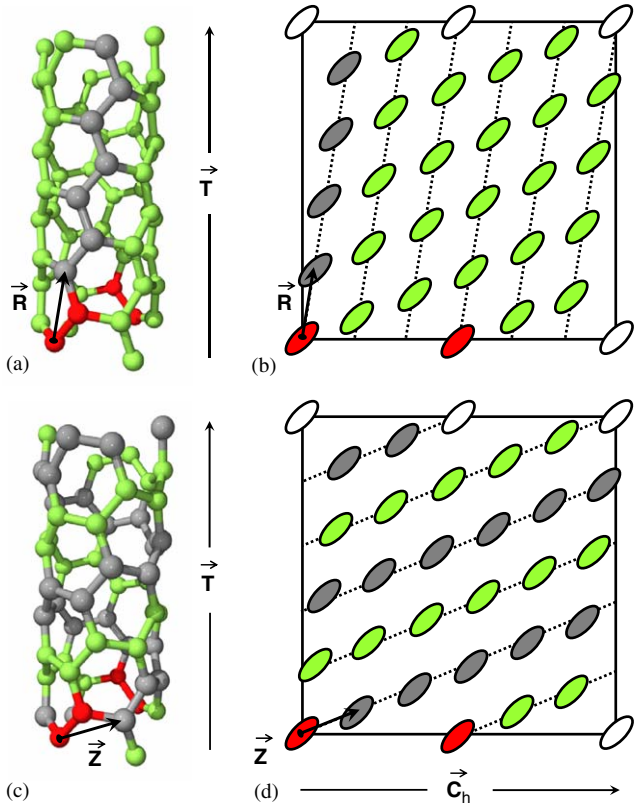

Fig. 6. Unit cell of the (4, 2) nanotube, with its 28 atoms colored for a better visualization of the linear–helical (a) and helical–angular (c) constructions from a 2-atom motif (dark atoms in the tubes). Diagrams for the unfolded unit cell of the (4, 2) nanotube where, for better visualization, the 2-atom motif is depicted as a filled ellipse. The dark grey atoms and ellipses represent those atoms in the unit cell which can be directly obtained by the application of the $\vec{R}$ vector, for (a) and (b), or by the vector $\vec{Z}$, for (c) and (d), while the light grey atoms can be obtained from the latter by applying other symmetry operations, such as the translation vector $\vec{T}$, for (a) and (b), or the rotations of $2\pi/d$, for (c) and (d) [3].

each of the N/u lines will be associated with a number of solutions of the Hamiltonian which are always a multiple of $2u$, and thus are equal to the number of atoms in the reduced unit cell, so that the number of solutions of the Hamiltonian can be invariant. Furthermore, N/u should be an integer, and therefore, the number of different possible choices of screw vectors that can be used to construct the nanotube is limited by the number of integer factors of N. By appropriately choosing the screw vector $\vec{t}_{u,v} = \vec{R}$, which will define a reduced unit cell with two atoms, the reciprocal space structure of the nanotube can be superimposed on that of a graphene layer and all the properties of the nanotube can be obtained from that of 2D graphite. Thus, the "zone-folding" scheme can be understood as an application of the compound operations of the nanotube. Fig. 7(a) shows the reciprocal space of the (4, 2) nanotube constructed using the linear–helical representation and choosing the vector $\vec{R}$. The reciprocal space lattice vectors for the (4, 2) nanotubes ($\vec{\kappa}_1 = 28\vec{K}_1$ and $\vec{\kappa}_2 = \vec{K}_2 - 6\vec{K}_1$) are shown in Fig. 7(a) as compared to the graphene reciprocal space. The 1st Brillouin zone, which is shown in dark-grey, can be translated to the adjacent Brillouin zones, shown in light-grey, by applying reciprocal lattice vectors.

2.4.3. Helical–angular construction

The helical–angular construction (see Fig. 4(c)) is obtained by choosing one of the screw vectors used to construct the nanotube to be parallel to $\vec{C}_h$. An obvious choice for that is the vector given by $\vec{C}_h/d$, where d is the greatest common divisor of n and m, thus dividing $\vec{C}_h = n\vec{a}_1 + m\vec{a}_2$ into integer units of $\vec{a}_1$ and $\vec{a}_2$. The other vector used to construct the nanotube can be any general screw vector, which can be written as $\{C_N^u | vT/N\}$. In the helical–angular construction, the screw vector plays the role of a generator of translations, while the vector in the circumferential direction generates

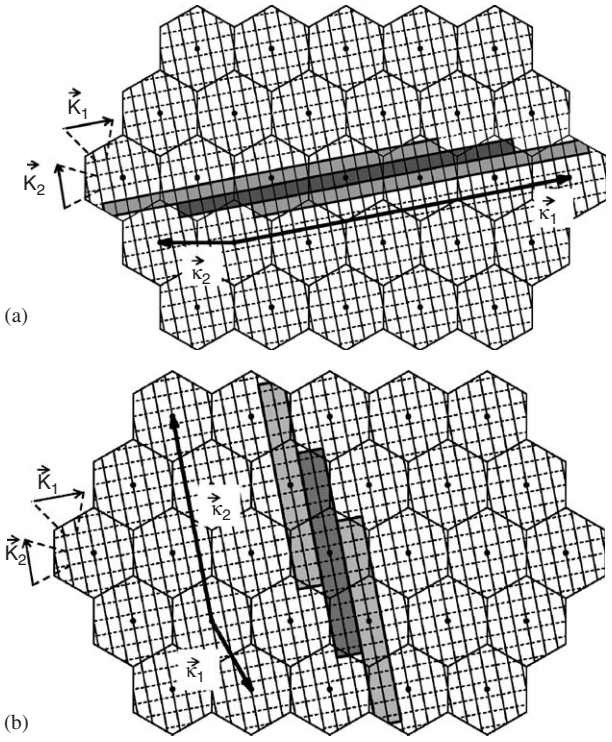

Fig. 7. Reciprocal space of the graphene layer. Parallel equidistant solid lines represent the cutting lines for the (4, 2) nanotube. The linear–helical (a) and helical–angular (b) 1st Brillouin zones are shown in dark-grey. The light grey rectangles are the Brillouin zones obtained by the unit vectors $\vec{\kappa}_2$ and $\vec{\kappa}_1$ of the linear–helical (a) and the helical–angular (b) reciprocal space structures, respectively [14].

pure rotations. This approach also allows the choice of a general screw vector for which the number of atoms in the reduced unit cell is 2, corresponding to the choice of a screw vector with $v = d$. In this case, u will follow the relation:

$$u = \frac{2n+m}{m}\frac{d}{d_R} + \frac{N}{m}q, \tag{14}$$

for which there will be $2d$ different values of q that lead to integer values of u. These vectors are equivalent, and therefore, to avoid confusion, the shortest vector should always be chosen. In their work, Damnjanović et al. defined the screw vector $\vec{Z}$, related to the quantity r, which is defined in Ref. [5]. The value r can be regarded as the number of times the nanotube is rotated by 2π when the vector $\vec{Z}$ is applied N times. In their publication, it was pointed out that any multiple of N/d could be added to r without causing any changes to the symmetry properties of the nanotube. This will result in d possible values for u. However, the values of u obtained with both $q \geqslant 0$ and $q < 0$ should be taken into account, and thus $2d$ choices of u can be used without loss of generality. In Fig. 4(c) we show again the 2-atom reduced unit cell for a (4, 2) nanotube. For this nanotube the smallest value $u = 5$ in the helical–angular construction can be obtained by choosing $q = 0$. The screw vector $\vec{Z}$ defined by Damnjanović et al. used $u = 9$ (or actually $u = -9$) for the (4, 2) nanotube which is obtained by choosing $q = -1$ in Eq. (14). This discrepancy originates from the fact that the arithmetical equation developed in Ref. [5] for obtaining the screw vectors only considered values of $q < 0$. It should be pointed out that the $\vec{Z}$ vector obtained here with $u = 5$ is equivalent to the one obtained by Damnjanović et al. [5] and the choice of one vector or another is only a matter of convention. As expected, the reduced unit cell also has a rhombic shape projected onto the cylindrical surface of the nanotube. However, in this case one side of the rhombus is aligned with the circumferential direction and has a magnitude of C_h/d while the other side coincides with the screw vector $\vec{Z}$. To help the visualization of the effect of the screw vector $\vec{Z}$, we show a diagram of the (4, 2) unit cell in Fig. 6(c). The vector $\vec{Z}$ was obtained using the smallest value of $u = 5$. The darker atoms represent a 2-atom motif, while the dark-grey helix represents the atoms in the unit cell which are obtained from the 2-atom motif by consecutive applications of the vector $\vec{Z}$. The light-grey atoms are obtained by applying the vector $\vec{C}_h/d$, $d = 2$ for the

(4, 2) nanotube, to one of the atoms in the dark-grey helix. For a better visualization, the diagram in Fig. 6(d) shows the unit cell of the (4, 2) nanotube unfolded, and with the 2-atom motif represented by an ellipse.

Considering that in the helical–angular construction one of the unit vectors is a general screw translation $\{C_N^u|vT/N\}$ and the other is the vector $\vec{C}_h/d$ in the circumferential direction, the reciprocal space vectors are found to be

$$\vec{\kappa}_1 = (d)\vec{K}_1 - (ud/v)\vec{K}_2 \tag{15}$$

and

$$\vec{\kappa}_2 = (N/v)\vec{K}_2. \tag{16}$$

In this formulation, the vector $\vec{\kappa}_2$ is parallel to the cutting lines, and thus the Brillouin zone of the nanotube can be defined as a rectangle formed by d cutting lines of length $(N/v)2\pi/T$. Each of the cutting lines will be associated with a number of solutions of the Hamiltonian which is a multiple of the number of atoms in the reduced unit cell $(2v/d)$. Each of the d lines can be associated with pure angular momenta while the points within the line will be associated with a helical momentum. By choosing a screw vector with $v = d$, the number of atoms in the reduced unit cell is 2, and therefore, the reciprocal space can be superimposed on that of a graphene layer. Fig. 7(b), shows the reciprocal lattice vectors $\vec{\kappa}_1 = 2\vec{K}_1 - 5\vec{K}_2$ and $\vec{\kappa}_2 = 14\vec{K}_2$ obtained for the (4, 2) nanotube from Eqs. (15) and (16).

It is important to note that, since the vector $\vec{C}_h/d$ is a finite symmetry operation and does not play the role of a translation in this construction, it is convenient to consider a different reduced unit cell which is composed of the $2d$ atoms. This reduced unit cell is obtained by applying the $\vec{C}_h/d$ operation on the original 2-atom motif, or equivalently by choosing the vector in the circumferential direction to be $\vec{C}_h$ instead of $\vec{C}_h/d$. By making this choice, the nanotube restores its quasi-1D-system character and the reduced unit cell can be represented by a cylinder of height given by Td/N which includes $2d$ atoms. The advantage of using this $2d$-atom reduced unit cell is the fact that it exhibits all the point group operations of the nanotube and the highest order symmetry operation is the rotation of $2\pi/d$ around the nanotube axis. Thus, the nanotube will have a 1D reciprocal lattice, spaced by a $2N\pi/(Td)$ length. The number of independent solutions of any nanotube property will be a multiple of $2d$. Since, in this case, the reduced unit cell has more than two atoms, the nanotube reciprocal space structure cannot be directly compared with that of a graphene layer.

2.4.4. Linear–angular construction

The last case is the linear–angular construction where the translation vector $\vec{T}$ and a vector parallel to $\vec{C}_h$ are used to construct the nanotube. In the case where the vector in the circumferential direction is chosen to be $\vec{C}_h/d$, the reduced unit cell is formed by one of the d sections of the nanotube translational unit cell, and thus it has $2N/d$ atoms. This construction can be regarded as a specific case of either the linear–helical or the helical–angular construction. Therefore, all the properties obtained generally for either of these two constructions independently should coincide as they approach the linear–angular case.

In the linear–angular construction, the unit vectors are $\vec{T}$ and $\vec{C}_h/d$. Thus the reciprocal space vectors $\vec{\kappa}_1$ and $\vec{\kappa}_2$ are given by:

$$\vec{\kappa}_1 = (d)\vec{K}_1 \tag{17}$$

and

$$\vec{\kappa}_2 = \vec{K}_2. \tag{18}$$

Since the number of atoms in the unit cell is $2N/d$, the reciprocal space structure of the nanotube, as defined here, cannot be mapped onto that of a graphene layer.

In the case where the vector in the circumferential direction is chosen to be the chiral vector $\vec{C}_h$, instead of $\vec{C}_h/d$, we restore the full nanotube unit cell, with a total of $2N$ atoms, as it was defined in Section 2.2. The nanotube can then be regarded as a 1D system, which will have a reciprocal lattice vector given by $\vec{K}_2$, as defined in Section 2.3, and thus the 1st Brillouin zone has a length $2\pi/T$.

3. Group theory for carbon nanotubes

As discussed in Section 2.4, chiral carbon nanotubes exhibit compound operations and therefore belong to non-symmorphic space groups. In this section we will start by developing the symmetry of a general chiral nanotube within

the framework of space group theory. The discussion is then extended to the more symmetric achiral (armchair and zigzag) carbon nanotubes, which are also non-symmorphic, due to the presence of glide planes. The space group theory presented here is based on the formalism of the group of the wavevector, which takes into consideration the full symmetry of the purely translational unit cell, which has $2N$ atoms and is compatible with the linear–angular construction. However, the linear–helical construction of the nanotube, in which the translational vector $\vec{T}$ and a general screw vector $\vec{t}_{u,v}$ are used to obtain the nanotube structure, also maintains the pure translational symmetry of the nanotube. Therefore, space group theory within the framework of the group of the wavevector is also compatible with the linear–helical construction. As we will show in Section 3.4, this compatibility allows for the direct comparison between the symmetry properties obtained from group theory and from the "zone-folding" scheme.

3.1. Symmetries for chiral carbon nanotubes

The chiral nanotube symmetry operations can be separated into two sets. The first set, which we shall call the symmorphic set, is formed by the translation operations of the nanotube and the point group operations. The symmorphic set forms a sub-group of the total space-group of the nanotube, and thus it can be used to obtain some of the symmetry-related properties. This group can be obtained as a weak direct-product [15] between the translational sub-group of the nanotube, composed of all the primitive translations, and the point group operations of the nanotube. To obtain the point group of the nanotube, we observe that in Section 2.4.4 we have shown that the nanotube can be rotated by an angle $2\pi/d$ without changing its structure. Therefore, the C_d operation is a point group operation of the nanotube. Also, by choosing an appropriate axis perpendicular to the nanotube axis, the rotation by π around this axis (C_2' or C_2'') will also be a symmetry operation of the nanotube (see Fig. 8(a)). There are two different classes of rotations perpendicular to the nanotube axis (C_2' and C_2''). For one of the classes (C_2'), the axis goes through the center of bonds between two equivalent atoms (shown in Fig. 8(a)). For the other class (C_2''), the axis goes through the centers of the hexagons. The point group of the nanotube can thus be obtained to be the axial point group D_d. In achiral nanotubes, besides the screw vectors, there are also mirror planes perpendicular to the nanotube axis and parallel to it, which are shown, respectively, in Figs. 8(b) and (c) for the (3, 3) nanotube.

The second set of symmetry operations, which we shall refer to as the non-symmorphic set, is formed by the compound operations of the space group of the nanotube, which cannot be decomposed into pure translations of multiples of $\vec{T}$ and point group operations. In the case of chiral nanotubes, all the screw vectors $\vec{t}_{u,v}$, with the exception of multiples of $\vec{T}$ and $\vec{C}_h/d$, are part of this set of operations. In achiral tubes, glide planes are also part of this set.

Crystalline structures (both symmorphic and non-symmorphic) are described by infinite groups since, ideally, these structures have an infinite number of translations. It is easier to work the group theory of finite groups, and thus, it is

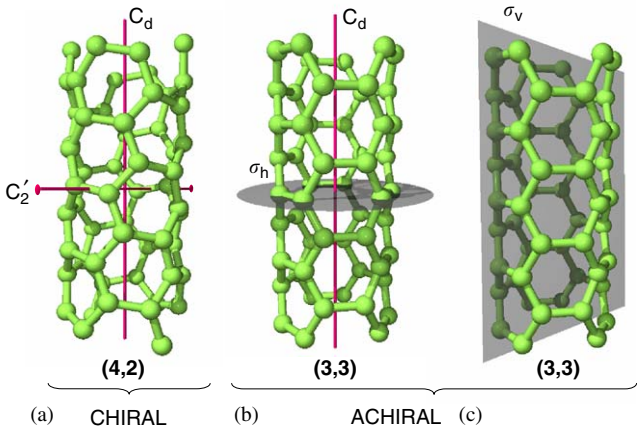

Fig. 8. (a) Unit cell of the chiral (4, 2) nanotube, showing the C_d, with $d = 2$, rotation around the nanotube axis and one of the C_2' rotations perpendicular to the tube axis. A different class of rotations (C_2''), which is also present for chiral and achiral nanotubes, is not shown here. (b) A section of an achiral armchair (3, 3) nanotube is shown with the horizontal mirror plane σ_h and the symmetry operation C_d, with $d = 3$. (c) The same (3, 3) armchair nanotube is shown with one of the vertical mirror planes σ_v.

necessary to factor out the translations by use of the concept of factor groups [8,16]. This concept is based on the fact that for any group G which has an invariant sub-group $\mathfrak{T}$, a factor group $G/\mathfrak{T}$ can be defined by separating the elements of G into cosets of $\mathfrak{T}$. Each coset of $\mathfrak{T}$ is going to act as an element of the factor group $G/\mathfrak{T}$, that is a finite group which can be isomorphic to a point group. In the case of materials exhibiting only symmorphic operations, the factorization is obvious and we end up with the point group of the space group (primitive translation $\tau = 0$) and its sub-groups. In contrast, for non-symmorphic structures, the factor group is usually not a sub-group of the space group. Therefore, the separation between the translation and the point group operations is not obvious and the factor group has to be found by obtaining the cosets of the translational sub-group $\mathfrak{T}$.

The group of the wavevector k for non-symmorphic space groups is obtained by defining the invariant subgroup $\mathfrak{T}_k$ of the primitive translations τ that follow the relation:

$$\exp(\mathrm{i}k\tau) = 1. \tag{19}$$

Note here, that both the wavevector k and the translation vector τ are being regarded as scalars, instead of vectors since all translations in nanotubes occur in the axial direction.

An arbitrary $k \neq 0$ can be written in the form $k = \pm\sigma\pi/\eta T$, where σ and η are both integers and coprime [17]. In this case, any vector of the form $\tau = \alpha\eta T$ will satisfy Eq. (19), with α being an arbitrary integer, and therefore will be an element of the subgroup $\mathfrak{T}_k$. In the cases of $k = 0$ and π/T, the invariant subgroup $\mathfrak{T}_k$ is exactly the group of all primitive translations of the nanotube which can be written as $\tau = \alpha T$, with α being an arbitrary integer.

The next step is to determine the different cosets of $\mathfrak{T}_k$ which are going to be the elements of the factor group and to organize them into classes. This can be done by observing two properties of cosets of invariant subgroups [18] which will not be proven here:

- Given two different symmetry elements (g_1 and g_2) of the group G, if there is at least one pair of elements of the invariant subgroup $\mathfrak{T}_k$ (τ_α and τ_β) which satisfy the condition: $g_1\tau_\alpha = g_2\tau_\beta$, then the cosets $g_1\mathfrak{T}_k$ and $g_2\mathfrak{T}_k$ are identical, and therefore it can be said that both g_1 and g_2 generate the same coset of $\mathfrak{T}_k$.
- Given two different cosets of the factor group $G/\mathfrak{T}_k$ generated by different elements of G (g_1 and g_2), if there is an element X of G for which $g_2 = X^{-1}g_1X$, the two cosets ($g_1\mathfrak{T}_k$ and $g_2\mathfrak{T}_k$) will belong to the same class in the factor group $G/\mathfrak{T}_k$.

3.1.1. Group of the wave vector at the Γ point ($k = 0$)

For easier comprehension, we will first obtain the factor group for $k = 0$, in which case the elements of $\mathfrak{T}$ can be written in the form $\tau_\alpha = \alpha T$.

Consider two arbitrary elements of a set of screw translations $\{C_N^u|vT/N\}$, $\{C_N^u|vT/N\}^2$, $\{C_N^u|vT/N\}^3\ldots$ which we will denote by $\{C_N^u|vT/N\}^s$ and $\{C_N^u|vT/N\}^l$. Taking the product between each of these elements with two arbitrary members of the invariant translational subgroup of the wavevector $k = 0$, namely $\{E|\alpha T\}$ and $\{E|\beta T\}$, we obtain

$$\{C_N^u|vT/N\}^s\{E|\alpha T\} = \{C_N^{su}|svT/N + \alpha T\}, \tag{20}$$

$$\{C_N^u|vT/N\}^l\{E|\beta T\} = \{C_N^{lu}|lvT/N + \beta T\}. \tag{21}$$

If there is at least one pair (α,β) which satisfies

$$\{C_N^{su}|svT/N + \alpha T\} = \{C_N^{lu}|lvT/N + \beta T\}, \tag{22}$$

then the cosets formed by the products $\{C_N^u|vT/N\}^s\mathfrak{T}$ and $\{C_N^u|vT/N\}^l\mathfrak{T}$ are identical.

Relation (22) will only be true if

$$l = s + \lambda N/u \tag{23}$$

and

$$sv/N + \alpha = lv/N + \beta, \tag{24}$$

Table 1
Character table for the group of the wavevectors $k = 0$ and π/T for chiral tubes. This group is isomorphic to the point group D_N

D_N	$\{E\|0\}$	$2\{C_N^u\|vT/N\}$	$2\{C_N^u\|vT/N\}^2$	...	$2\{C_N^u\|vT/N\}^{(N/2)-1}$	$\{C_N^u\|vT/N\}^{N/2}$	$(N/2)\{C_2'\|0\}$	$(N/2)\{C_2''\|0\}$
A_1	1	1	1	...	1	1	1	1
A_2	1	1	1	...	1	1	-1	-1
B_1	1	-1	1	...	$(-1)^{(N/2-1)}$	$(-1)^{N/2}$	1	-1
B_2	1	-1	1	...	$(-1)^{(N/2-1)}$	$(-1)^{N/2}$	-1	1
E_1	2	$2\cos 2\pi/N$	$2\cos 4\pi/N$	...	$2\cos 2(N/2-1)\pi/N$	-2	0	0
E_2	2	$2\cos 4\pi/N$	$2\cos 8\pi/N$	...	$2\cos 4(N/2-1)\pi/N$	2	0	0
⋮	⋮	⋮	⋮	⋮	⋮	⋮	⋮	⋮
$E_{(N/2-1)}$	2	$2\cos 2(N/2-1)\pi/N$	$2\cos 4(N/2-1)\pi/N$	...	$2\cos 2(N/2-1)^2\pi/N$	$2\cos(N/2-1)\pi$	0	0

where λ is an integer. Substituting for the value of l, we obtain:

$$\lambda v = (\alpha - \beta)u. \tag{25}$$

Since α and β can assume any integer values, it is always possible to find a pair of values for which the difference is an integer multiple of v, namely $\alpha - \beta = \lambda' v$. Substituting this relations back into the value of l in Eq. (23), we obtain

$$l = s + \lambda' N, \tag{26}$$

where λ' is an arbitrary integer. Therefore, l and s have N independent values $(1, \ldots, N)$ and the factor group of chiral nanotubes will have N distinct cosets related to the screw axis operation. Each of these cosets can be associated with one of the screw translations of order N which, in turn, is associated with specific lattice vectors of the graphene layer. The space group of the nanotube should not depend on the choice of the screw vector. It can be easily shown that any choice of screw vectors of order N will yield the same cosets.

To obtain the full symmetry of the factor group of the wavevector $k = 0$ we also have to consider the point group symmetries, and how they can form classes. It can be shown that the C_2' and C_2'' rotations perpendicular to the nanotube axis generate two independent cosets $\{C_2'|0\}\mathfrak{T}$ and $\{C_2''|0\}\mathfrak{T}$, each belonging to a different class. Also, these symmetry operations take the screw operation $\{C_N^u|vT/N\}^s$ into $\{C_N^{-u}| - vT/N\}^s = \{C_N^u|vT/N\}^{-s} \equiv \{C_N^u|vT/N\}^{N-s}$. In general, these two operations (s and $-s$) will originate different cosets, with the exception of the cases where $s = 0$ and $N/2$. Using the second property in Section 3.1, it can be shown that C_2' and C_2'' operations make the cosets of s and $-s$ belong to the same class. $s = 0$ will generate the same coset as the identity and $s = N/2$ and $-N/2$ will generate the same coset, and the class to which this coset belongs has only one element. It should be emphasized that N is always even, and therefore $N/2$ is always an integer.

Finally, it is necessary to show the effect of the primitive rotational operation (C_d), which is a symmetry operation in nanotubes where $d = gcd(n, m)$ is larger than 1. The rotational symmetry in this case is a d-fold axis C_d which brings the arbitrary screw translation $\{C_N^{lu}|lvT/N\}$ into $\{C_N^{lu+N/d}|lvT/N\}$. The operation $\{C_d|0\}$ generates the same coset as the screw vector $\{C_N^u|vT/N\}^{N/d}$, and thus, it does not increase the symmetry of the nanotubes any further.

We can conclude that the symmetry of the factor group is isomorphic to the D_N point group, for which the character table is shown in Table 1. However, it is important to mention that although the factor group of chiral nanotubes is isomorphic to D_N, the symmetry operations of the nanotube may be different from the symmetry elements of the D_N point group. The C_N^s symmetry operations in the D_N point group correspond to the cosets of the screw operations $\{C_N^u|vT/N\}^s\mathfrak{T}$. In the same way, the C_2' and C_2'' operations correspond to the cosets $\{C_2'|0\}\mathfrak{T}$ and $\{C_2''|0\}\mathfrak{T}$, respectively. Thus, it is clear that each of the representations of the D_N group can be labeled with a quantum number $\tilde{h}$, which should be associated with a helical momentum. The nature of this helical quantum number $\tilde{h}$ will be discussed in more detail in Section 3.4.

3.1.2. Group of the wave vector at a general point ($0 < k < \pi/T$)

For $k \neq 0$ one must find the star of k, which is the set of wavevectors that are obtained by carrying out all the point group operations on the wavevector k [8]. The rotational symmetry of chiral nanotubes (C_d) will not affect the values of

k in the axial direction, and therefore the symmetry operation C_d has no effect on the star of k. However, it is clear that the presence of a perpendicular axis C_2' takes $-k$ into k and, therefore, the star of k will include both the positive and the negative value of k. Thus, it is only necessary to find the group of the wavevector k for either positive or negative values of k. For simplicity, we shall only consider positive values of k. The group of the wavevector k is the group of all symmetry operations which leave k invariant or takes k to an equivalent value (different by a primitive translation in reciprocal space). Rotations around the nanotube axis will leave k invariant, and thus will be part of the group of the wavevector k. However, in the case of $0 < k < \pi/T$, the C_2' and C_2'' operations do not leave k invariant, and therefore they should not be considered symmetry operations the group of the wavevector k. To obtain the factor group of the wavevector k, it is convenient to write k as $\pi\sigma/\eta T$ with σ and η being coprimes, as introduced in Section 3.1. We then write the elements of the translational subgroup of the wavevector k, $\mathfrak{T}_k$, in the form $\{E|\alpha\eta T\}$, with α being an arbitrary integer and E being the identity operation. The value η represents the number of unit cells of the nanotube which have to be spanned so that the modified Bloch relation in Eq. (19) is satisfied for $k \neq 0$.

We can repeat the same procedure of Section 3.1.1 to find the symmetry of the factor group for $k \neq 0$. The product between two elements $\{C_N^u|vT/N\}^s$ and $\{C_N^u|vT/N\}^l$ of a set of screw vectors with two arbitrary members of the invariant translational subgroup of the wavevector $k > 0$, namely $\{E|\alpha\eta T\}$ and $\{E|\beta\eta T\}$ will only be equal if

$$l = s + \lambda N/u \tag{27}$$

and

$$sv/N + \alpha\eta = lv/N + \beta\eta, \tag{28}$$

which leads to $\lambda v = (\alpha - \beta)u\eta$. As before, α and β can assume any integer values, and therefore there can always be a pair (α,β) which satisfies: $\alpha - \beta = \lambda' v$, for λ' being an integer. This leads to the relation

$$l = s + \lambda'\eta N. \tag{29}$$

The group of the wavevector at $0 < k < \pi/T$ is, therefore, isomorphic to a $C_{\eta N}$ point group, which is Abelian and has each symmetry element in a class by itself. The only point group operation of k in the axial direction is the rotational operation C_d, which, as we have shown in Section 3.1.1, does not increase the symmetry of the factor group any further. The $C_{\eta N}$ point group has ηN 1D irreducible representations. However, it can be shown that due to the compatibility relations between two arbitrary wavevectors k, the only irreducible representations of this group which can be related to solutions of the Hamiltonian are the ones which transform as the representations of the C_N point group. The extra representations originate from a usual result in the factor group analysis of the group of the wavevector, that is the generation of irrelevant representations related to pure translations [8]. Thus, for any physical problem, the symmetry properties of nanotubes for $0 < k < \pi/T$ can be fully described by using a factor group which is isomorphic to C_N. In Table 2, we show the character table for the representations of the C_N point group. Note that from the N irreducible representations of the C_N group, there are $(N/2 - 1)$ representations which are doubly degenerate due to time reversal symmetry. These representations are in fact 1D and to differentiate them from the 2D irreducible representations of the D_N group we use different fonts in Tables 2 and 1 to label the representations.

The case of $k = \pi/T$, known as the X point in the Brillouin zone boundary [3], can be obtained by considering $\sigma = \eta = 1$ and including the C_2' and C_2'' symmetry operations, since the $k = \pi/T$ and $-\pi/T$ can be translated into each other by a reciprocal lattice vector $\kappa_2 = 2\pi/T$. Thus, because of the presence of the C_2 symmetry operations, the group of the wavevector at $k = \pi/T$ is also isomorphic to D_N.

For example, in the case of the (4, 2) nanotube shown in Fig. 8(a), where $N = 28$, the group of the wavevector at a general point $0 < k < \pi/T$ is isomorphic to the D_{28} point group and the number of irreducible representations and of classes is 28, and while at $k = 0$ and π/T the group of the wavevector is isomorphic to C_{28} and the number of irreducible representations and classes is 13.

3.2. Group theory for achiral carbon nanotubes

The group theory of achiral nanotubes can be obtained in a similar manner as was done for chiral tubes in Sections 3.1.1 and 3.1.2. Both armchair (n, n) and zigzag $(n, 0)$ carbon nanotubes exhibit all the symmetry operations that were observed for chiral nanotubes, namely the screw axes $\{C_N^u|vT/N\}^s$, where $N = 2n$, the rotation around the nanotube

Table 2
Character table for the group of the wavevector $0 < k < \pi/T$ for chiral tubes[a]

C_N	$\{E\|0\}$	$\{C_N^u\|vT/N\}^1$	$\{C_N^u\|vT/N\}^2$	$\cdots$	$\{C_N^u\|vT/N\}^\ell$	$\cdots$	$\{C_N^u\|vT/N\}^{N-1}$
A	1	1	1	$\cdots$	1	$\cdots$	1
B	1	-1	1	$\cdots$	$(-1)^\ell$	$\cdots$	-1
$\mathbb{E}_{\pm 1}$	$\left\{\begin{matrix}1\\1\end{matrix}\right.$	$\begin{matrix}\epsilon\\ \epsilon^*\end{matrix}$	$\begin{matrix}\epsilon^2\\ \epsilon^{*2}\end{matrix}$	$\cdots$	$\begin{matrix}\epsilon^\ell\\ \epsilon^{*\ell}\end{matrix}$	$\cdots$	$\left.\begin{matrix}\epsilon^{N-1}\\ \epsilon^{*(N-1)}\end{matrix}\right\}$
$\mathbb{E}_{\pm 2}$	$\left\{\begin{matrix}1\\1\end{matrix}\right.$	$\begin{matrix}\epsilon^2\\ \epsilon^{*2}\end{matrix}$	$\begin{matrix}\epsilon^4\\ \epsilon^{*4}\end{matrix}$	$\cdots$	$\begin{matrix}\epsilon^{2\ell}\\ \epsilon^{*2\ell}\end{matrix}$	$\cdots$	$\left.\begin{matrix}\epsilon^{2(N-1)}\\ \epsilon^{*2(N-1)}\end{matrix}\right\}$
$\vdots$	$\vdots$	$\vdots$	$\vdots$	$\vdots$	$\vdots$	$\vdots$	$\vdots$
$\mathbb{E}_{\pm(\frac{N}{2}-1)}$	$\left\{\begin{matrix}1\\1\end{matrix}\right.$	$\begin{matrix}\epsilon^{\frac{N}{2}-1}\\ \epsilon^{*\frac{N}{2}-1}\end{matrix}$	$\begin{matrix}\epsilon^{2(\frac{N}{2}-1)}\\ \epsilon^{*2(\frac{N}{2}-1)}\end{matrix}$	$\cdots$	$\begin{matrix}\epsilon^{\ell(\frac{N}{2}-1)}\\ \epsilon^{*\ell(\frac{N}{2}-1)}\end{matrix}$	$\cdots$	$\left.\begin{matrix}\epsilon^{(N-1)(\frac{N}{2}-1)}\\ \epsilon^{*(N-1)(\frac{N}{2}-1)}\end{matrix}\right\}$

[a]This group is isomorphic to the point group C_N. The $\pm$ signs label the different 1D representations ($\mathbb{E}$) with characters which are complex conjugates of each other. These representations are degenerate due to time reversal symmetry. The complex number ϵ is $e^{i2\pi/N}$ and ϵ^* is the complex conjugate of ϵ.

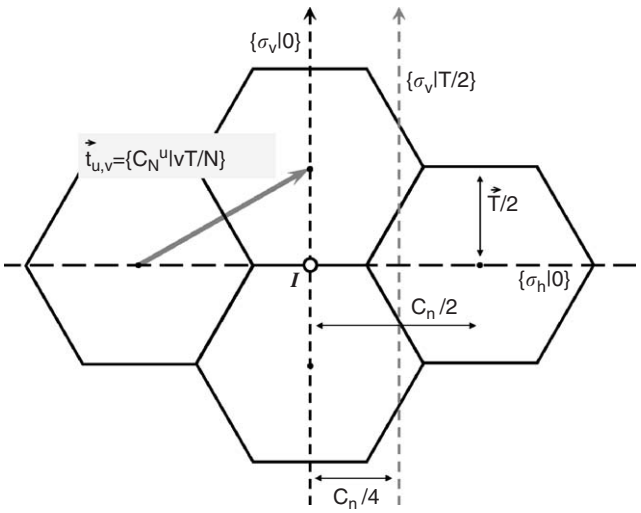

Fig. 9. Extra symmetry operations of an armchair achiral nanotube. Short-dashed arrows correspond to vertical mirror planes (heavy dashes) and glide planes (light dashes) and the horizontal long-dashed line corresponds to a horizontal mirror plane. The solid arrow corresponds to the screw vector which is also present in achiral tubes. The large open dot indicates the position of an inversion center I [6,7].

axis C_d, where $d = n$, and the rotations perpendicular to the nanotube axis C_2' and C_2''. However, achiral nanotubes also exhibit other symmetry operations such as inversion centers, mirror planes and glide planes. The horizontal mirror plane σ_h and one of the vertical mirror planes σ_v are shown in Figs. 8(b) and (c), respectively. There is also an inversion center at the intersection of the σ_h plane and the nanotube axis. The glide planes, which can be represented as $\{\sigma_v|T/2\}$, are shown schematically in Fig. 9 for an armchair nanotube.

To obtain the factor group of the wavevector $k = 0$, it is necessary to obtain all the non-equivalent cosets of the translational subgroup $\mathfrak{T}$, and then to separate them into classes, in the same way that is done for point groups [8]. It is known from Section 3.1.1 that the factor group of the wavevector $k = 0$ exhibits all the symmetry operations of the group D_{2n}, since for achiral tubes $N = 2n$. The other symmetries of the nanotube can be obtained from the direct product group $D_{2n} \otimes C_{1h}$ which results in a group which is isomorphic to D_{2nh}. The same point group was obtained by Alon for the rod [19] group of achiral nanotubes [6,7] for which the screw vectors were written in terms of improper axes S_{2n}. The character tables for the D_{2nh} group is shown in Table 3, where the C_{2n} classes correspond to screw vectors of the nanotube, while the σ_v' and σ_v'' classes correspond, respectively, to mirror and glide planes containing the nanotube axis.

Table 3
Character table for the group of the wavevectors $k = 0$ and π/T for achiral tubes[a]

D_{2nh}	$\{E\|0\}$	$\cdots$	$2\{C_{2n}^{u}\|vT/2n\}^{s}$	$\cdots$	$\{C_{2n}^{u}\|vT/2n\}^{n}$	$n\{C_2'\|0\}$	$n\{C_2''\|0\}$	$\{I\|0\}$	$\cdots$	$2\{IC_{2n}^{u}\|vT/2n\}^{s}$	$\cdots$	$\{\sigma_h\|0\}$	$n\{\sigma_v'\|0\}$	$n\{\sigma_v''\|T/2\}$
A_{1g}	1	$\cdots$	1	$\cdots$	1	1	1	1	$\cdots$	1	$\cdots$	1	1	1
A_{2g}	1	$\cdots$	1	$\cdots$	1	-1	-1	1	$\cdots$	1	$\cdots$	1	-1	-1
B_{1g}	1	$\cdots$	$(-1)^s$	$\cdots$	-1	1	-1	1	$\cdots$	$(-1)^s$	$\cdots$	-1	1	-1
B_{2g}	1	$\cdots$	$(-1)^s$	$\cdots$	-1	-1	1	1	$\cdots$	$(-1)^s$	$\cdots$	-1	-1	1
$\vdots$	$\vdots$	$\vdots$	$\vdots$	$\vdots$	$\vdots$	$\vdots$	$\vdots$	$\vdots$	$\vdots$	$\vdots$	$\vdots$	$\vdots$	$\vdots$	
$E_{\mu g}$	2	$\cdots$	$2\cos(\mu s\pi/n)$	$\cdots$	$2(-1)^{\mu}$	0	0	2	$\cdots$	$2\cos(\mu s\pi/n)$	$\cdots$	$2(-1)^{\mu}$	0	0
$\vdots$	$\vdots$	$\vdots$	$\vdots$	$\vdots$	$\vdots$	$\vdots$	$\vdots$	$\vdots$	$\vdots$	$\vdots$	$\vdots$	$\vdots$	$\vdots$	$\vdots$
A_{1u}	1	$\cdots$	1	$\cdots$	1	1	1	-1	$\cdots$	-1	$\cdots$	-1	-1	-1
A_{2u}	1	$\cdots$	1	$\cdots$	1	-1	-1	-1	$\cdots$	-1	$\cdots$	-1	1	1
B_{1u}	1	$\cdots$	$(-1)^s$	$\cdots$	-1	1	-1	-1	$\cdots$	$-(-1)^s$	$\cdots$	1	-1	1
B_{2u}	1	$\cdots$	$(-1)^s$	$\cdots$	-1	-1	1	-1	$\cdots$	$-(-1)^s$	$\cdots$	1	1	-1
$\vdots$	$\vdots$	$\vdots$	$\vdots$	$\vdots$	$\vdots$	$\vdots$	$\vdots$	$\vdots$	$\vdots$	$\vdots$	$\vdots$			
$E_{\mu u}$	2	$\cdots$	$2\cos(\mu s\pi/n)$	$\cdots$	$2(-1)^{\mu}$	0	0	-2	$\cdots$	$-2\cos(\mu s\pi/n)$	$\cdots$	$-2(-1)^{\mu}$	0	0
$\vdots$	$\vdots$	$\vdots$	$\vdots$	$\vdots$	$\vdots$	$\vdots$	$\vdots$	$\vdots$	$\vdots$	$\vdots$	$\vdots$	$\vdots$	$\vdots$	$\vdots$

[a]This group is isomorphic to the point group D_{2nh}. The values of s and μ span the integer values between 1 and $n-1$.

Table 4
Character table for the group of the wavevectors $0 < k < \pi/T$ for achiral tubes[a]

C_{2nv}	$\{E\|0\}$	$2\{C_{2n}^{u}\|vT/2n\}^{1}$	$\{C_{2n}^{u}\|vT/2n\}^{2}$	...	$2\{C_{2n}^{u}\|vT/2n\}^{n-1}$	$\{C_{2n}^{u}\|vT/2n\}^{n}$	$n\{\sigma_v'\|0\}$	$n\{\sigma_v''\|T/2\}$
A'	1	1	1	...	1	1	1	1
A''	1	1	1	...	1	1	-1	-1
B'	1	-1	1	...	$(-1)^{(n-1)}$	$(-1)^n$	1	-1
B''	1	-1	1	...	$(-1)^{(n-1)}$	$(-1)^n$	-1	1
E_1	2	$2\cos\pi/n$	$2\cos 2\pi/n$	...	$2\cos 2(n-1)\pi/n$	-2	0	0
E_2	2	$2\cos 2\pi/n$	$2\cos 4\pi/n$	...	$2\cos 4(n-1)\pi/n$	2	0	0
$\vdots$	$\vdots$	$\vdots$	$\vdots$	$\vdots$	$\vdots$	$\vdots$	$\vdots$	$\vdots$
$E_{(n-1)}$	2	$2\cos(n-1)\pi/n$	$2\cos 2(n-1)\pi/n$	...	$2\cos(n-1)^2\pi/n$	$2\cos(n-1)\pi$	0	0

[a]This group is isomorphic to the point group C_{2nv}.

For $0 < k < \pi/T$ the only symmetry operations which maintain k invariant are the screw vectors and the mirror and glide planes which contain the nanotube axis (σ_v' and σ_v''). The factor group of the wavevector k will then be isomorphic to the C_{2nv} point group, for which the character table is shown in Table 4.

In the case of the (3, 3) nanotube (see Figs. 8(b) and (c)), the group of the wavevector at a general point $0 < k < \pi/T$ is isomorphic to the C_{6v} point group while at $k = 0$ and π/T the group of the wavevector is isomorphic to the D_{6h} point group.

3.3. Eigenvectors and the irreducible representations

Having the irreducible representations of the wavevector k, it is possible to obtain the symmetries of the eigenvectors used to describe the electronic and vibrational properties for all the points of the first Brillouin zone. The first Brillouin zone of the nanotube will extend from $k = -\pi/T$ to π/T. According to space group theory, for each point k in the 1st Brillouin zone, the eigenvectors will have a symmetry which is given by one of the irreducible representations of the group of the wavevector k. Therefore, we can associate each solution of the Hamiltonian which transforms as the space group of the nanotube with an irreducible representation $\mathscr{D}_{\mu}(k)$ of the group of the wavevector k, and therefore we can label the solution with the quantum numbers k and μ, and the wavefunction can be denoted by $\psi_{\mu}(k)$.

Table 5
Compatibility relations between the irreducible representations of the D_N and C_N groups, where $\mu = 1 \ldots (N/2 - 1)$

C_N $0 < k < \pi/T$	D_N $k = 0, \pi/T$
A	A_1
	A_2
B	B_1
	B_2
$\mathbb{E}_{\pm\tilde{\mu}}$	$E_{\tilde{\mu}}$

Table 6
Compatibility relations between the irreducible representations of the D_{2nh} and C_{2nv} groups, where $\mu = 1 \ldots (N/2 - 1)$

C_{2nv} $0 < k < \pi/T$	D_{2nh} $k = 0, \pi/T$
A'	A_{1g}
	A_{2u}
A''	A_{1u}
	A_{2g}
B'	B_{1g}
	B_{2u}
B''	B_{1u}
	B_{2g}
E_μ	$E_{\mu g}$
	$E_{\mu u}$

As shown in Section 3.1.2, for the case of chiral nanotubes, the representations at $0 < k < \pi/T$ will be given by group C_N. In the C_N group there are N 1D irreducible representations, from which $N - 2$ representations are brought together in pairs ($\mathbb{E}_{\tilde{\mu}}$ and $\mathbb{E}_{-\tilde{\mu}}$) by time reversal symmetry making $-k$ to be equivalent to k. The remaining symmetries A and B differ in relation to their parity on the application of the screw vector $\{C_N^u|vT/N\}^s$, for s odd. At $k = 0$ and π/T, there are four 1D representations and $[(N/2) - 1]$ 2D representations. The 1D representations A_1 and A_2 differ regarding parity with respect to the C_2' and C_2'' operations, which exchange the two inequivalent atoms in the 2-atom reduced unit cell. The same difference applies to the B_1 and B_2 irreducible representations. The compatibility relations between the group of the wavevector at $k = 0$ and at $k = \pi/T$ (D_N) and at $k \neq 0$ (C_N) are summarized in Table 5.

In the case of achiral tubes, the factor group of the wavevector $0 < k < \pi/T$ is isomorphic to C_{2nv}, which has four 1D-representations and $(n - 1)$ 2D-representations. In this group, the B representations are related to states which are antisymmetric upon the application of the screw vector $\{C_N^u|vT/N\}^s$ with s odd, while the A representations relate to the corresponding symmetric states. The representations with a single prime ($'$) are related to states which are symmetric under the σ_v operation, while the double prime representations ($''$) are antisymmetric under the same set of operations. At $k = 0$ and π/T, the factor group is isomorphic to the D_{2nh} point group. The D_{2nh} group has eight 1D representations and $(2n - 2)$ 2D representations. The 1D representations are labeled by $A_{1(g,u)}$, $A_{2(g,u)}$, $B_{1(g,u)}$ and $B_{2(g,u)}$. Again, A and B differ in parity with respect to the application of the screw vector, while the subscripts 1 and 2 are related to the parity under rotations perpendicular to the nanotube axis (C_2' and C_2''), 1 for even and 2 for odd. The u and g subscripts are related to the parity upon the inversion of the coordinate system. The compatibility relations between the representations of the D_{2nh} and the C_{2nv} groups are summarized in Table 6.

3.4. Quantum numbers and crystal momentum

As explained in Section 3.1.1, the quantum number that labels the irreducible representations of the factor group of the wavevector k is associated with a helical momentum labeled by a helical quantum number $\tilde{h}$ which can be understood in

terms of an helical coordinate ξ. The variable ξ specifies the position on a helicoidal orbit around the nanotube cylinder which can be defined so that it follows two conditions: first, that any point on the cylinder that delimits the nanotube can be determined by the z coordinate along the nanotube axis and the coordinate ξ. Second, that the application of the screw operation $\{C_N^u|vT/N\}$, used to construct the nanotube, changes only the coordinate ξ, leaving the coordinate z invariant. In this sense, the helical wavevector $\tilde{h}$ can be associated with a helical momentum which will be conserved. However, to avoid the discomfort of working with helical coordinates, it is possible to use only the projection of this coordinate in the direction of the pure rotations of the nanotube, and to disregard its translational component. In this case, the helical quantum number is reduced to its angular projection, denoted as $\tilde{\mu}$, which is not a conserved quantity when crossing the Brillouin zone boundary, but still can be used to label the irreducible representations.

We can understand the nature of the quantum number $\tilde{\mu}$ by comparing it to the reciprocal lattice vectors in the linear–helical construction of the nanotube structure (see Section 2.4.2). Within this construction, the nanotube structure in reciprocal space is obtained from the reciprocal lattice vectors $\vec{\kappa}_1 = (N/u)\vec{K}_1$ and $\vec{\kappa}_2 = \vec{K}_2 - (v/u)\vec{K}_1$, where $\vec{K}_1$ and $\vec{K}_2$ are the reciprocal lattice vectors of the nanotube structure as defined in Section 2.3. Since the reciprocal lattice vector $\vec{K}_1$ can only assume integer values of $2\pi/C_h$, for a given value of k along the cutting lines, there are N/u inequivalent values of $\tilde{\mu}$. In the case of a 2-atom reduced unit cell, obtained for $u = 1$ within this construction, each of the N inequivalent cutting lines can be directly associated with one of the N irreducible representations of the factor group of the wavevector k (for chiral tubes). Therefore, we have a direct relation between the quantum number $\tilde{\mu}$ and the cutting line indices which have been referred to in the literature as μ [3]. It is important to emphasize that this connection can only be obtained by choosing the 2-atom reduced unit cell. Following this approach, the linear quantum number k can be directly associated with $\vec{K}_2$, since both originate from the translational symmetry vector $\vec{T}$. However, it should be noted that if the value of k crosses the boundary of the 1st Brillouin zone, it is necessary to use the vectors $\vec{\kappa}_1$ and $\vec{\kappa}_2$ to translate it back to the 1st Brillouin zone (see Fig. 7). By doing this, the quasi-angular momentum $\tilde{\mu}$ will be corrected by a multiple of v/u, which, in the case of the 2-atom unit cell is denoted by the quantity M. This correction arises from the fact that $\tilde{\mu}$ is only a projection of the helical quantum number $\tilde{h}$, and it will be of great importance for the evaluation of the selection rules in the case where the operator couples k states in different Brillouin zones. This will happen in the case of double resonance Raman scattering processes and in the formation of excitonic eigenstates, which will be discussed in Sections 7.3 and 8.1, respectively. For most cases, the selection rules for the interaction between two different k, $\tilde{\mu}$ states will be easily obtained directly from the conservation of linear momenta on the graphene reciprocal lattice structure, in terms of the cutting lines (see Section 7.4) [14]. This approach has been widely used in the literature and is useful for better physical understanding. The limitations of the cutting lines approach for obtaining the selection rules appear when the group of the wavevector k is of higher symmetry, such as at $k = 0$ for chiral tubes and at any value of k for achiral tubes. In this case, the selection rules for the coupling between states of different parity, such as A and B symmetry states or $E_{\mu g}$ and $E_{\mu u}$ states, cannot be obtained from the cutting lines approach. Thus, although many of the selection rules can be obtained from the conservation of momentum in the "unfolded" graphene layer, this approach is not complete and in many cases it has to be refined by a more detailed analysis.

4. Line groups vs. group of the wavevector

The symmetry of systems exhibiting translational periodicity in one dimension, such as stereoregular polymers and carbon nanotubes, have been described in terms of line groups [4,20]. Also, some three-dimensional crystals can be highly anisotropic, as for example ferromagnetic and ferroelectric systems, chain-type crystals, and these crystals have line groups as subgroups of their space groups. Whenever only one direction is relevant for some physical properties of a three-dimensional system, one can expect to derive useful information by applying suitable line groups only. Line groups are infinite groups for which the irreducible representations contain all the symmetry properties of the material in 1 direction.

Line groups can be represented as a weak-direct product $L = Z \cdot P$, where Z and P are, respectively, the *generalized* translation group and the axial point group symmetry of the system. The product must be a weak-direct product [15] (indicated here by "$\cdot$") because all elements of Z, except for the identity, have a nonzero translational part, while no point group element in P has translations. The intersection is, therefore, only the identity operation [21]. Thus, the main difference between the formalism used in Section 3 and the formalism which will be presented here is the fact that, within the framework of the group of the wavevector k, the infinite translational part of the space group operations is factored out, and the remaining operations are viewed as "generalized" point group operations, while in the line group

formalism, the point group operations, and the remaining operations are viewed as "generalized" translations, forming an infinite group. The line groups are then constructed as a weak-direct [15] product between the point group and the group of generalized translations.

It is important to notice that the axial point group P has to be composed solely of symmetry operations which maintain the line axis invariant, and we will conveniently choose the line axis to be the z axis. Therefore, the *axial* point groups P can be: C_n, S_{2n}, C_{nh}, C_{nv}, D_n, D_{nh} and D_{nd}, where $n = 1, 2, 3, \ldots$ is the order of the principal rotation axis. There are two types of axial point groups, those for which all operations leave a point z along the axis invariant and those for which there is at least one operation in the group which takes z into $-z$ [4].

By the *generalized* translation group, we mean that group Z denotes infinite cyclic groups composed of general translational operations along the line axis, and these operations may include screw axes or glide planes. The symmetry elements of Z can be represented by $\{R|\tau\}$, where R is either a rotation C_N^u of u times $2\pi/N$ around the nanotube axis or a mirror plane which contains the line axis (σ_v), while τ is a translation vT/N along the line axis of a fraction of the translational vector of the system denoted by $\vec{T}$. In the case of the glide plane $vT/N = T/2$. The values of u and v are integers, which in the case of nanotubes will be defined as in Eqs. (5) and (6). There are three different types of generalized translation groups:

- Those formed by simple translations, $T = \{E|T\}$. The translational period is T;
- Those with the occurrence of a screw axis, $T_N^u = \{C_N^u|vT/N\}$. The translational period is vT;
- Those with the occurrence of a glide plane, $T_c = \{\sigma_v|T/2\}$. The translational period is $T/2$.

However, a product $Z \cdot P$ forms a group only if Z and P commute (this is always the case only for $Z = T$). Furthermore, some products with different factors are identical. There is an infinite number of line groups, and they are classified into 13 families [21]. The line group of chiral nanotubes belongs to the family $\mathbf{L}N_v2$ or $\mathbf{L}N_v22$ depending on whether d is even or odd. The $\mathbf{L}N_v2$ and $\mathbf{L}N_v22$ families of line groups, as defined in Ref. [20], can be factorized as $T_N^u \cdot D_d$, where D_d is the point group of the chiral nanotubes. For achiral nanotubes, the line group will belong to the family denoted by $\mathbf{L}2d_d/mcm$ which can be factorized as $T_{2d} \cdot D_{dh}$ [20,21]. In Ref. [21], a table of all the 13 families is shown together with their respective factorizations. It should be noted that, for the sake of consistency within our work, the symbols used here to label the different families are different from the symbols used in Ref. [21]. Also, the irreducible representations for all the line group families are described in the literature [22,23]. For clarity, we will obtain here the irreducible representations of the line group of chiral carbon nanotubes from the properties of the "generalized" translational group. The line group approach can only be applied using the pure translational group, which will lead to irreducible representations and quantum numbers equivalent to those obtained using the approach of the group of the wavevector [24]. The results obtained in this section will be used later for a comparison between the line group formalism and the formalism of the group of the wavevector for obtaining the symmetry-related properties of carbon nanotubes.

4.1. Line group of chiral carbon nanotubes

In this section, we will derive the line group of chiral carbon nanotubes using the formalism first developed by Vujičić et al. [20]. The corresponding derivation for achiral nanotubes follows the same pattern and will not be shown here. To construct the line group for chiral carbon nanotubes, it is necessary to first define the group of *generalized* translations Z. In the case of chiral nanotubes, the group Z can be obtained by choosing one of the general screw vectors of the nanotube which, as defined in Section 2.4, can be written as $\{C_N^u|vT/N\}$. It will not be explicitly shown here, but any choice of screw vector of the nanotube will yield line groups which belong to the same family. We can construct the irreducible representations of the line group of *generalized* translations by writing the wavefunctions in terms of (ξ, φ), where the helical coordinate ξ is defined so that $\{C_N^u|vT/N\}^s\xi = \xi + 2\pi s$ and φ is a rotation around the nanotube axis. The irreducible representations of the generalized translational group should then obey a modified Bloch relation:

$$\{C_N^u|vT/N\}^s\psi(\xi, \varphi) = \psi(\xi + 2\pi s, \varphi) = \exp(\mathrm{i}\tilde{h}\xi)\psi(\xi, \varphi) = \psi(\xi, \varphi). \tag{30}$$

Thus the irreducible representations of the line group of screw translations $\{C_N^u|vT/N\}$ will be written as

$$_{\tilde{h}}\mathscr{T} = \exp(\mathrm{i}\tilde{h}\xi), \tag{31}$$

where the notation ${}_{\tilde{h}}\mathscr{T}$ is introduced to avoid confusion with the space group notation $\mathscr{T}_k$. Note that, in this notation, the quantum number related to the generalized translation appears as a subscript on the left-hand side of the character which labels the representation ($\mathscr{T}$). In this purely helical formulation, the quantum number $\tilde{h}$, which is a helical wavevector that can only be represented in two dimensions, is completely conserved. The variables ξ and φ can be written in terms of cylindrical coordinates z and ϕ and thus the irreducible representations will be obtained in terms of the projections of $\tilde{h}$ on the translational and rotational parts ($\tilde{k}$ and $\tilde{\mu}$) as

$$ {}_{\tilde{k}}\mathscr{T}_{\tilde{\mu}}(\{C_N^u|vT/N\}^s) = \exp\left[\mathrm{i}\tilde{k}\frac{svT}{N} + \mathrm{i}\tilde{\mu}\frac{2\pi su}{N}\right]. \tag{32} $$

However, in this notation, neither the pure translation $\{E|vT/N\}$ nor the pure rotation $\{C_N^u|0\}$ are symmetry operations of the nanotube. Thus the quantum numbers that label the irreducible representations, $\tilde{k}$ and $\tilde{\mu}$, are not conserved separately. By using Eq. (32), the modified Bloch relation for the wavefunctions, given by Eq. (30) can be rewritten in terms of z and ϕ:

$$ \{C_N^u|vT/N\}^s\psi(z,\phi) = \psi\left(z + \frac{svT}{N}, \phi + \frac{2\pi su}{N}\right) = \exp\left[\mathrm{i}\left(\tilde{k}\frac{svT}{N} + \tilde{\mu}\frac{2\pi su}{N}\right)\right]\psi(z,\phi) = \psi(z,\phi), \tag{33} $$

where the value of $\tilde{k}$ varies within the range of $(-N\pi/(vT), N\pi/(vT)]$, while $\tilde{\mu}$ assumes integer values between $-N/(2u)+1$ and $N/(2u)$, provided that u is a divisor of $N/2$.

Since we are constructing the irreducible representation of the translational group, it is convenient to take only the translational projection of $\tilde{h}$. This projection assumes the values of $\tilde{k}$ which vary from $[-N\pi/(vT), N\pi/(vT)]$. It should be noted that in Section 3.4, the same coordinate ξ was introduced to obtain the irreducible representations of the space group of nanotubes. Note that in the formulation of the group of the wavevector, the angular projection of $\tilde{h}$ was used to label the representations (see Section 3.4).

To obtain the irreducible representations of the line group of chiral nanotubes, it is necessary to apply the operations of the axial point group of the nanotube to the irreducible representations of the group Z. The axial point group of chiral nanotubes is the D_d group, where d is defined in Section 2 as $d = gcd(n, m)$. The D_d point group can be represented as $D_d = C_d + C_2'C_d$ where C_d is the Abelian group of the d-fold rotations around the z axis and C_2' is a rotation perpendicular to the z axis. The irreducible representations of the group of the nanotube can also be obtained by first getting the irreducible representations of the product $Z \cdot C_d$ and then constructing the final representations by applying $Z \cdot D_d = Z \cdot C_d + C_2'(Z \cdot C_d)$.

The irreducible representations of the group are easily obtained from $Z \cdot C_d$, where Z is the group of screw translations. The operations of C_d leave any point on the z axis invariant. Therefore, the representations of $Z \cdot C_d$ will be obtained by multiplying the representations of Z, given in Eq. (32), by the irreducible representations of group C_d. The point group C_d is an Abelian group in which all representations are 1D. The μth representation of the symmetry operation C_d^l of group C_d is given by $\Gamma_\mu(C_d^l) = \exp(\mathrm{i}l\mu 2\pi/d)$, where l and μ can assume integer values between 0 and d. Here, μ labels the representations of the nanotube point group, and is related to pure rotations, in contrast with $\tilde{\mu}$, which is a projection of $\tilde{h}$.

The representations of the group $Z \cdot C_d$ will then be given by

$$ {}_{\tilde{h}}\mathscr{D}_\mu(C_d^l\{C_N^u|vT/N\}) = \exp\left[\mathrm{i}\tilde{h}\xi + \mathrm{i}\mu l\frac{2\pi}{d}\right], \tag{34} $$

where ${}_{\tilde{h}}\mathscr{D}_\mu$ is used to denote the irreducible representations of line groups. Here, $\tilde{h}$ and μ are quantum numbers labeling these representations. It is convenient to use only the projection of $\tilde{h}$ in the translational direction ($\tilde{k}$) in the representations, ignoring the rotational part ($\tilde{\mu}$). Thus, the representations will be written as

$$ {}_{\tilde{k}}\mathscr{D}_\mu(\{C_N^{u+Nl/d}|vT/N\}) = \exp\left[\mathrm{i}\tilde{k}\frac{vT}{N} + \mathrm{i}\mu l\frac{2\pi}{d}\right]. \tag{35} $$

However, it can be understood that the C_2' symmetry operation not only takes z to $-z$, but also causes the two intrinsically different screw vectors $\{C_N^u|vT/N\}^s$ and $\{C_N^u|vT/N\}^{-s}$ to be equivalent and therefore they should have the same irreducible representation, and thus belong to the same class. Note that for $k \neq 0$ the representations

${}_{\tilde{k}}\Gamma_{\mu}(\{C_N^{u+lN/d}|vT/N\}^s)$ and ${}_{\tilde{k}}\Gamma_{\mu}(\{C_N^{u+lN/d}|vT/N\}^{-s})$ are complex conjugates of each other, and thus they are of the same irreducible representation. Therefore, to construct the representations of the group $Z \cdot D_d$ it is necessary to reorganize the representations for either $\tilde{k}$ or μ different from zero into 2-dimensional representations. The procedure for the construction of these representation is described in the work of Vujičić et al. and Bozović et al. [20,22,23]. These representations will then assume the form

$$ {}^{-\tilde{k}}_{\tilde{k}}E_{\mu}^{-\mu}(\{C_N^{u+lN/d}|vT/N\}^s) = \begin{pmatrix} \epsilon & 0 \\ 0 & \epsilon^* \end{pmatrix}, \tag{36} $$

and

$$ {}^{-\tilde{k}}_{\tilde{k}}E_{\mu}^{-\mu}(\{C_2C_N^{u+lN/d}|vT/N\}^s) = \begin{pmatrix} 0 & \epsilon^* \\ \epsilon & 0 \end{pmatrix}, \tag{37} $$

where $\epsilon = \exp(\mathrm{i}s\tilde{k}vT/N + \mathrm{i}s\mu l 2\pi/d)$, and the notation ${}^{-\tilde{k}}_{\tilde{k}}E_{\mu}^{-\mu}$, with the left-hand side super and subscripts, is introduced to differentiate this line group representation from the notation used for the representations of the group of the wavevector k, which are labeled only by $\tilde{\mu}$ as a subscript on the right-hand side. For $\tilde{k} = 0$ and $\mu = 0$, we have $\epsilon = \epsilon^* = 1$ and the representations ${}^0_0E_0^0$ will be reducible. Therefore, these representations will be rewritten as 1D representations ${}_0A_0^+$ and ${}_0A_0^-$, where the "+" and "−" signs refer to the parity of the representation upon the C_2' operation, "+" for even and "−" for odd. The notation ${}_0A_0$ is also introduced to differentiate it from the A symmetries used for the irreducible representations of the group of the wavevector. The subscripts 0 indicate that the labels $\tilde{k}$ and μ are both equal to zero. The same happens for $\tilde{k} = N\pi/(vT)$ and $\mu = 0$, for which the irreducible representations will be rewritten as ${}_{N\pi/(vT)}A_0^+$ and ${}_{N\pi/(vT)}A_0^-$.

A similar procedure can be used to construct the line group of achiral nanotubes, which will belong to the $\mathbf{L}2d_d/mcm$ family. The irreducible representations, Bloch functions and selection rules for chiral and achiral nanotubes are described in detail in the literature [25].

4.2. Eigenvectors and the irreducible representations

In space group theory, the representations of the translation group are obtained of the pure translational symmetry, and thus are independent of the rotations of the system. Therefore, as is common in group theory, the irreducible representations of this translation group are all 1D and do not have any influence on the dimension of the irreducible representations of the factor group. In contrast, in the line group formalism, the generator of translations is a screw vector, which also applies a rotation to the system. Thus, the separation between rotations and translations is not completely achieved. The representations of the line group are not specifically of rotations or translations, but a mixture of both. Although only the projection of the helical wavevector $\tilde{h}$ is used to label the representations, the representations have to reflect the mixed character between the translational and rotational operations. Therefore, the representations of the group of "generalized" translations will have some properties of point group representations. For example, the symmetry operation C_2' takes all translations τ in the z direction to $-\tau$ and all rotations by ϕ around the z axis to rotations by $-\phi$. In the line group formalism, the screw vectors $\{R_{\phi}|\tau\}$ and $\{R_{-\phi}|-\tau\} \equiv \{R_{\phi}|\tau\}^{-1}$ will belong to the same class and have the same characters for each irreducible representation.

The relation between irreducible representations and the eigenvectors within the line group formalism becomes more clear if we take into consideration the $2d$-atom reduced unit cell introduced in Section 2.4.3. The $2d$-atom reduced unit cell exhibits all the symmetry of the nanotube, and can be regarded as a "generalized" unit cell, from which the nanotube is constructed by successive applications of a "generalized" translation. Thus, there will be a multiple of $2d$ independent solutions to a Hamiltonian with the nanotube symmetry. For chiral nanotubes there are d 2D irreducible representations for $0 < \tilde{k} < N\pi/(vT)$. Thus, each of the d representations will be associated with two different eigenstates, one eigenstate related to bonding states and one to anti-bonding states, in a similar fashion to that discussed in Section 3.3. At $\tilde{k} = 0$ there are two 1D irreducible representations (namely, ${}_0A_0^+$ and ${}_0A_0^-$) and also two 1D representations for $\tilde{k} = N\pi/(vT)$ (namely, ${}_{N\pi/(vT)}A_0^+$ and ${}_{N\pi/(vT)}A_0^-$). In these representations the "+" signs are related to bonding states while the "−" signs can be associated with anti-bonding states, as in Section 3.3.

Within the line group approach, both helical momentum and angular momentum conservation will arise directly from the selection rules. Thus, the formalism of line groups is very convenient when there is a coupling between states

Table 7
Quantum numbers used to label the irreducible representations in the line group and in the group of the wavevector formalisms

Quantum number	Symmetry	Group theory	Range
k	Translational	Wavevector	$(-\pi/T, \pi/T]$
μ	Rotational	Line	$0, \ldots, d-1$
$\tilde{h}\left\{\begin{array}{l}\tilde{k}\\ \tilde{\mu}\end{array}\right.$	Translational	Line	$[0, \pi N/(dT)]$
	Rotational	Wavevector	$1-N/2, \ldots, N/2$

The helical quantum number ($\tilde{h}$) can be used in either of the formalisms. However, the use of its projections $\tilde{k}$ and $\tilde{\mu}$ is more common.

which are associated with different linear and angular momentum quantum numbers. However, it should be noted here that the formalism of the group of the wavevector yields the same symmetry-related properties, and the choice of the formalism is more dependent on the acquaintance of the researcher with one of the formalisms than on any intrinsic difference between them. In Section 5.1 we will compare the results for the group of the wavevector and for line groups regarding the symmetry of electronic states.

4.3. Quantum numbers and crystal momentum

The irreducible representations of the line group of nanotubes are labeled by the quasi-linear quantum number $\tilde{k}$ and the angular momentum quantum number μ. The fact that the quasi-linear wavevector $\tilde{k}$ is not a conserved quantity comes directly from its definition as the translational projection of the helical quantum number $\tilde{h}$. This case is opposite to that of the group of the wavevector, for which the label k corresponds to a pure linear quantum number and $\tilde{\mu}$ is the angular projection of $\tilde{h}$. In Table 7, we show a summary of the quantum numbers used to label the irreducible representations of line groups and the group of the wavevector, specifying where each quantum number can be applied and what is the range of inequivalent values that each quantum number can assume.

To better comprehend the conservation of the quasi-linear quantum number $\tilde{k}$ and of the angular momentum μ, we follow the same procedure as was used in Section 3.4 and we compare the quantum numbers $\tilde{k}$ and μ with the lattice vectors $\vec{\kappa}_1$ and $\vec{\kappa}_2$ for the 2-atom unit cell with the helical–angular reciprocal space structure. As shown in Section 2.4.3, the nanotube lattice vectors will be given by $\vec{\kappa}_1 = d\vec{K}_1 + (ud/v)\vec{K}_2$ and $\vec{\kappa}_2 = N/dK_2$, with $v = d$. Thus, for a given cutting line μ, the inequivalent values of K_2 lie in the $(0, (N/d)\pi/T)$ range. Each representation of the line group of chiral nanotubes labeled by $\tilde{k}$ and μ can be associated with different points of the "unfolded" reciprocal space of the nanotube. In the case when the quantum numbers $\tilde{k}$ and μ exceed the limits of the 1st Brillouin zone of the helical–angular reciprocal space, it is necessary to use the reciprocal lattice vectors $\vec{\kappa}_1$ and $\vec{\kappa}_2$ to translate them back into the 1st Brillouin zone. This reciprocal space operation corrects the quasi-linear wavevector by a multiple of u. The correction of the quasi-linear quantum number $\tilde{k}$ also arises from the fact that this quantum number is only a projection of the helical quantum number $\tilde{h}$. As in the group of the wavevector formalism, this correction will affect the evaluation of the selection rules for coupling between states from different Brillouin zones. In this sense, the approach of using the cutting lines to evaluate the selection rules may prove to be more convenient, although, it should always be followed by a more detailed analysis to determine if the parity of the eigenstates influences the selection rules. For this part of the analysis, the researcher can choose between the line group formalism and that of the group of the wavevector, whichever he (she) finds more convenient.

5. Electronic band structure

For large diameter nanotubes ($d_t > 1.5$ nm) the electronic band structure can be derived from that of a flat graphene layer by using the concept of cutting lines [14]. Using the zone-folding scheme, the electronic band structure of the nanotube can be easily obtained by superimposing the cutting lines in the linear–helical representation of reciprocal space on the band structure of a graphene layer. The two carbon atoms A and B per unit cell of the graphene layer (see Fig. 2) have one free π-electron each, resulting in the appearance of the valence and conduction bands in the electronic band structure of the graphene layer, where the valence π band corresponds to a bonding state between the two atoms, and the conduction π^* band corresponds to an anti-bonding state. The valence and conduction bands are degenerate at the K and K' points in reciprocal space, which occur at the Fermi level (see Fig. 10(a)), while the other electronic

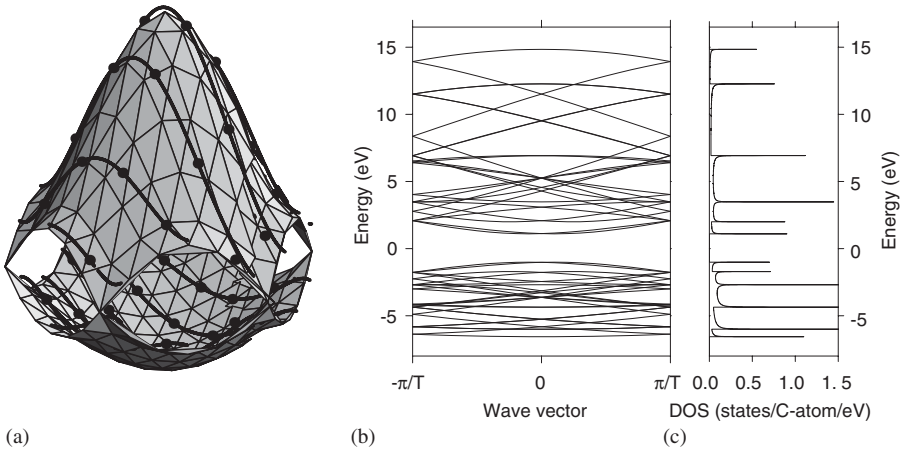

Fig. 10. (a) The conduction and valence bands of the graphene layer in the first Brillouin zone calculated according to the π-band nearest-neighbor tight-binding model. Solid curves show the cutting lines for the (4, 2) nanotube. Solid dots show the ends of the cutting lines in the 2-atom linear–helical representation. (b) Electronic energy band diagram for the (4, 2) nanotube obtained by zone-folding from (a). (c) Density of electronic states for the electronic energy band diagram shown in (b) [14].

energy bands correspond to sp^2-hybridized electrons involved in covalent bonds, and these sp^2 electrons lie far away in energy from the Fermi level.

The energy–momentum contours for the valence and conduction bands of the graphene layer in the first Brillouin zone, calculated by using the π-band nearest-neighbor tight-binding approximation [3], are shown in Fig. 10(a). The solid curves plotted in Fig. 10(a) on the energy–momentum contours indicate the cutting lines for our (4, 2) sample nanotube. The solid dots stand for the ends of the cutting lines obtained from the 2-atom linear–helical construction, for which $u = 1$ and $v = M = 6$, which we translated to the 1st Brillouin zone for a better visualization. Following the zone-folding scheme, we now place the $E(\mathbf{k})$ dispersion along all the cutting lines from Fig. 10(a) in the one-dimensional Brillouin zone of the (4, 2) nanotube, as shown in Fig. 10(b). The corresponding density of electronic states (DOS) for the energy band diagram in Fig. 10(b) is shown in Fig. 10(c). One can clearly observe the presence of spikes, or van Hove singularities (VHSs), in the DOS of the (4, 2) nanotube in Fig. 10(c). The electronic structure of the (4, 2) nanotube is shown here only for illustrative purposes, since for small diameter nanotubes ($d_t < 0.6$ nm), the nanotube curvature mixes σ and π bands, and thus, the zone-folding scheme does not apply.

The total number of cutting lines in the 2-atom linear–helical construction of reciprocal space is equal to the number of hexagons in the nanotube translational unit cell, N (Section 2.4.2). Therefore, by superimposing N cutting lines on the two energy–momentum contours of the valence and conduction bands in the two-dimensional reciprocal space of the graphene layer (see Fig. 10(a)), one will obtain $2N$ electronic energy subbands in the one-dimensional reciprocal space of the nanotube (see Fig. 10(b)). Since there are two atoms per unit cell in the graphene layer, the total number of atoms in the nanotube unit cell is $2N$. Therefore, the total number of electronic energy subbands in the one-dimensional reciprocal space of the nanotube is equal to the total number of atoms in the nanotube unit cell, in agreement with the fact that there is one free π-electron per sp^2-hybridized carbon atom. It is possible to relate each of the cutting lines in chiral nanotubes (and thus each of the energy bands) to an irreducible representation of the factor group of nanotubes for a general point k. This factor group is isomorphic to C_N, and therefore has N 1D irreducible representations. For this reason, the cutting line index relates perfectly with the quasi-angular quantum number $\tilde{\mu}$ which labels the irreducible representations in the space group formalism. In this sense, the cutting lines with index $\tilde{\mu} = 0$ and $N/2$ can be associated with the A and B symmetry states, respectively. Since each cutting line is associated with two different energy bands, one in the valence band and one in the conduction band of the graphene band structure, each irreducible representation will also label two different eigenfunctions. At $k = 0$ the number of irreducible representations is changed to $N/2 + 2$ due to the fact that the $(N - 2)$ $\mathbb{E}$ representations of the C_N group become doubly degenerate. The A symmetry representation in the valence band will become an A_1 representation, following the symmetry of the graphene valence band at the center of the Brillouin zone, while the A symmetry representation in the conduction band will become an A_2 representation [3].

Table 8
Irreducible representations for the electronic conduction and valence bands of chiral and achiral nanotubes

		Valence		Conduction	
		$k=0,\pi/T$	$0<k<\pi/T$	$k=0,\pi/T$	$0<k<\pi/T$
Chiral	$\tilde{\mu}=0$	A_1	A	A_2	A
	$0<\tilde{\mu}<N/2$	$E_{\tilde{\mu}}$	$\mathbb{E}_{\pm\tilde{\mu}}$	$E_{\tilde{\mu}}$	$\mathbb{E}_{\pm\tilde{\mu}}$
	$\tilde{\mu}=N/2$	B_1	B	B_2	B
Armchair	$\tilde{\mu}=0$	A_{1g}	A'	A_{2g}	A''
	$0<\tilde{\mu}<n$	$E_{\tilde{\mu}g}$	$E_{\tilde{\mu}}$	$E_{\tilde{\mu}u}$	$E_{\tilde{\mu}}$
	$\tilde{\mu}=n$	B_{1g}	B'	B_{2g}	B''
Zigzag	$\tilde{\mu}=0$	A_{1g}	A'	A_{2u}	A'
	$0<\tilde{\mu}<n$	$E_{\tilde{\mu}u,\tilde{\mu}g}$ [a]	$E_{\tilde{\mu}}$	$E_{\tilde{\mu}g,\tilde{\mu}u}$ [a]	$E_{\tilde{\mu}}$
	$\tilde{\mu}=n$	B_{1g}	B'	B_{2u}	B'

[a]For zigzag nanotubes, if $\tilde{\mu}<2n/3$ the valence (conduction) band at $k=0$ belongs to the $E_{\tilde{\mu}g}$ ($E_{\tilde{\mu}u}$) representation for $\tilde{\mu}$ even and $E_{\tilde{\mu}u}$ ($E_{\tilde{\mu}g}$) for $\tilde{\mu}$ odd, while if $\tilde{\mu}>2n/3$ the its the opposite.

In the case of achiral nanotubes, the factor group for $0<k<\pi/T$ is isomorphic to the group C_{2nv}, for which the character table is given in Table 4. This group has $(n+2)$ irreducible representations, from which four are 1D and $(n-1)$ are 2D. The cutting lines with opposite indices $+\tilde{\mu}$ and $-\tilde{\mu}$, for $\tilde{\mu}$ varying from 1 to $(n-1)$, will be associated with the same 2D irreducible representation labeled by $\tilde{\mu}$. The conduction and valence bands associated with the same index $0<\tilde{\mu}<n$ will have the same symmetry $E_{\tilde{\mu}}$. The $\tilde{\mu}=0$ cutting line will cross the Γ point of the graphene layer and thus will be associated with A symmetry states, while the cutting line with $\tilde{\mu}=n$ will be associated with B symmetries. For armchair tubes, the anti-bonding states which constitute the conduction band will have A'' and B'' symmetries, for $\tilde{\mu}=0$ and n, respectively, while the valence band will be associated with A' and B' states. For zigzag nanotubes, the σ_v operation does not exchange the adjacent atoms, and thus both valence and conduction bands have A' and B' representations at $0<k<\pi/T$, where A' states correspond to the cutting lines with index $\tilde{\mu}=0$ and B' states correspond to $\tilde{\mu}=n$. To obtain the symmetries of the valence and conduction bands for both zigzag and armchair nanotubes at $k=0$, for which the group of the wavevector is isomorphic to D_{2nh}, it is necessary to apply the compatibility relations in Table 6. For zigzag nanotubes, eigenstates at $k=0$ in the valence (conduction) band associated with cutting line index $\tilde{\mu}<2n/3$ belong to irreducible representations which are even (odd) under the σ_h mirror operation, which exchanges the A and B atoms. However, cutting lines with index $\tilde{\mu}>2n/3$ are out of the first Brillouin zone in the unfolded (graphene) reciprocal space, and thus a phase shift causes an exchange in the parity of the $k=0$ eigenfunctions under the σ_h operation. The irreducible representations of the electronic states of chiral nanotubes and achiral nanotubes are summarized in Table 8.

The cutting line approach has been successfully used to predict the metallic or semiconducting nature of the nanotubes. Since the graphene valence and conduction bands cross at the K and K' points in the Brillouin zone, carbon nanotubes for which one of the cutting lines crosses the K or K' points should have a metallic behavior. In contrast, carbon nanotubes for which none of the cutting line passes through the K or K' points, show a band gap, and thus show semiconducting behavior. The cutting lines in the vicinity of the K point are shown in Fig. 11 for three different cases, $\mathrm{mod}(2n+m,3)=0$, $\mathrm{mod}(2n+m,3)=1$, and $\mathrm{mod}(2n+m,3)=2$. The first case, $\mathrm{mod}(2n+m,3)=0$, corresponds to the cutting line crossing the K point, resulting in metallic behavior, as discussed above. However, it has been reported that only armchair nanotubes are pure metallic nanotubes, whereas the other tubes for which the cutting lines cross the K and K' points are, in fact, tiny gap semiconductors [13,25–28]. Kleiner et al. used a simple model based on the π band nearest neighbor tight-binding approximation to explain these results based on symmetry-breaking between bonding and anti-bonding states in the valence and conduction bands due to the curvature of the nanotube [28].

This effect can be understood in terms of group theory. For both the valence and the conduction bands in chiral nanotubes, the cutting lines which cross the K and K' points are associated with the same representation $\mathbb{E}_{\mu}$. Therefore, the valence and conduction bands cannot cross at the Fermi energy, and the nanotube has to exhibit a small band gap [25]. For armchair nanotubes, the bands which cross the K and K' points are the bands associated with $\tilde{\mu}=n$ and thus have B' (valence band) and B'' (conduction band) symmetries. Since these bands

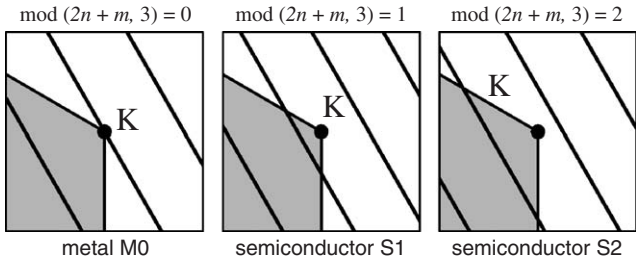

Fig. 11. Three different configurations of the cutting lines in the vicinity of the K point. The first configuration $\mathrm{mod}(2n+m,3)=0$ corresponds to the case of metallic nanotubes $M0$, and the last two configurations, $\mathrm{mod}(2n+m,3)=1$ and $\mathrm{mod}(2n+m,3)=2$, correspond to the case of semiconducting nanotubes of types $S1$ and $S2$, respectively [12].

have different symmetries, group theory does not forbid them to cross, and thus the presence of a mini-gap is not necessary.

The two cases of semiconducting nanotubes, $\mathrm{mod}(2n+m,3)=1$ and $\mathrm{mod}(2n+m,3)=2$, are also different from each other, depending on which side of the K point (K to Γ or K to M), in the unfolded two-dimensional Brillouin of a graphene sheet, the first VHS (van Hove singularity) in the DOS appears. We classify these two types of semiconducting nanotubes as $S1$ and $S2$, respectively. In a similar fashion, we can classify metallic nanotubes by what ratio the K point divides the cutting line in the 2-atom linear–helical representation. By projecting the vector $\vec{K}$ on the direction $\vec{K}_2$, one can find $(\vec{K}\cdot\vec{K}_2)/(\vec{K}_2\cdot\vec{K}_2)=m/d_R$. Thus, we can classify metallic nanotubes as $M1$ and $M2$ for $d_R=d$ and $d_R=3d$, correspondingly (see Section 2.2) [29]. For $M1$ metallic nanotubes, $m/d_R=m/d$ is an integer and therefore the K point appears at the wave vector $k=0$ in the one-dimensional Brillouin zone of the nanotube (the Γ point). For $M2$ metallic nanotubes, $m/d_R=(m/d)/3$ is one third of an integer, and therefore the K point appears at the wave vector $k=\pm(2/3)(\pi/T)$ in the one-dimensional Brillouin zone of the nanotube (two thirds of the distance from the central Γ point to the edge, X point, of the one-dimensional Brillouin zone). While armchair nanotubes (n,n) are always $M2$ type metallic tubes, and zigzag nanotubes can be either $M1$ type metallic $(3\ell,0)$ or $S1$ type $(3\ell+1,0)$ or $S2$ type $(3\ell+2,0)$ semiconducting tubes, while chiral nanotubes can be of each of the four types, $M1$, $M2$, $S1$, or $S2$. See Ref. [29] for more information on the classification of different types of nanotubes.

Although these considerations could be obtained in view of the simple "zone-folding" procedure, the symmetry of nanotubes, as described here, can be used to obtain the electronic band structure of carbon nanotubes within the approximations of the extended tight-binding model [11,12]. In fact, Samsonidze et al. used extended tight-binding calculations to obtain the electronic transition energies considering the structural relaxation that becomes significant in small diameter nanotubes [12]. The symmetry-adapted extended tight-binding model was able to obtain the dependence of the electronic transitions on the nanotube geometrical structure which could fit the experimental results with great accuracy [12]. However, a constant energy difference was found between the experimental and calculated results, which could be attributed to many-body corrections [30]. In Fig. 12 we show the electronic energy band structure of a (4, 2) nanotube, calculated using the extended tight-binding model.

5.1. Symmetry of electronic states from the line group approach

For a better comprehension of the relation between the group of the wavevector and the line group approaches, we will now discuss the symmetry of the electronic bands of chiral nanotubes from the standpoint of line groups. As explained in Section 4.2, each of the 2D irreducible representations can be associated with two different states, one for bonding states, which is related to the valence band, and one for anti-bonding states, related to the conduction band. In the case of $\tilde{k}=0$ and $\tilde{\mu}=0$, there are two 1D representations ${}_0A_0^+$ and ${}_0A_0^-$. Thus, the states in the valence band will be associated with the ${}_0A_0^+$ representation, while the states in the conduction band will have ${}_0A_0^-$ symmetry. These representations are equivalent to the A_1 and A_2 representations obtained for $k=0$ in space group theory. At $\tilde{k}=N\pi/(vT)$ there are also two 1D-representations, ${}_{N\pi/(vT)}A_0^+$ and ${}_{N\pi/(vT)}A_0^-$, which will be associated with the valence and conduction bands, respectively. Again, the relation between these symmetries and the B_1 and B_2 symmetries obtained at $k=\pi/T$ in space group theory is obvious. However, the representation of the line groups for a general wavevector $\tilde{k}$ cannot be

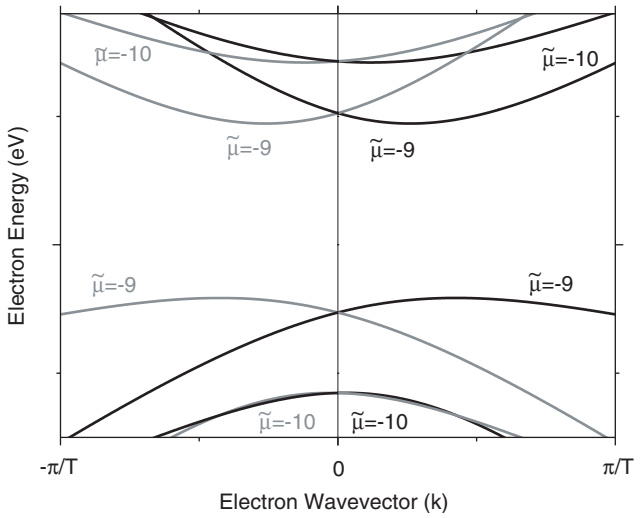

Fig. 12. Electronic bands for a (4, 2) nanotube, calculated using an extended tight-binding model [12], for the conduction and valence band states with quantum number $\tilde{\mu} = \pm 9$ and $\tilde{\mu} = \pm 10$. For clarity, the bands with negative indices ($\tilde{\mu}$) are shown by grey lines.

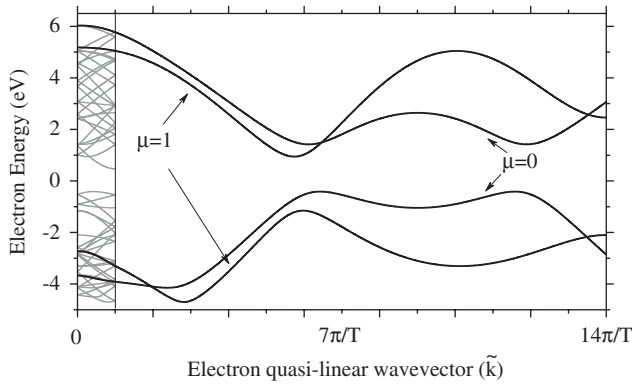

Fig. 13. Band structure of a (4, 2) nanotube for a $2d$-atom reduced unit-cell calculated using an extended tight-binding model. Also shown on the left is the electronic band structure for the $2N$-atom unit cell [12].

directly related to representations of the group of the wavevector k, since for these values of $\tilde{k}$ the translational part of the symmetry operation cannot be factored out of the representation. To obtain the relation between the representations obtained from the line group formalism and that of the group of the wavevector, it is necessary to consider the total helical quantum number $\tilde{h}$.

As an example, in Fig. 13 we show the band structure of a (4, 2) chiral nanotube for the $2d$-atom reduced unit cell (see Section 2.4.3). As discussed above, each $\tilde{k}$-point on these electronic bands will be associated with a representation of the line group of chiral nanotubes labeled by the quantum numbers $\tilde{k}$ and μ. The band structure for the $2N$-atom unit cell can be obtained by "folding" the band structure of the $2d$-atom unit cell, as shown on the left-hand side of Fig. 13. This "folding" process can be understood from Section 2.4.3 as a change from the helical–angular construction to the linear–angular construction (Section 2.4.4).

6. Phonons in carbon nanotubes

The phonon dispersion relations of the graphene layer can be calculated within a force constant model, or by ab initio methods [31–34]. Two atoms A and B in the unit cell of the graphene layer (see Fig. 2) give rise to six phonon branches,

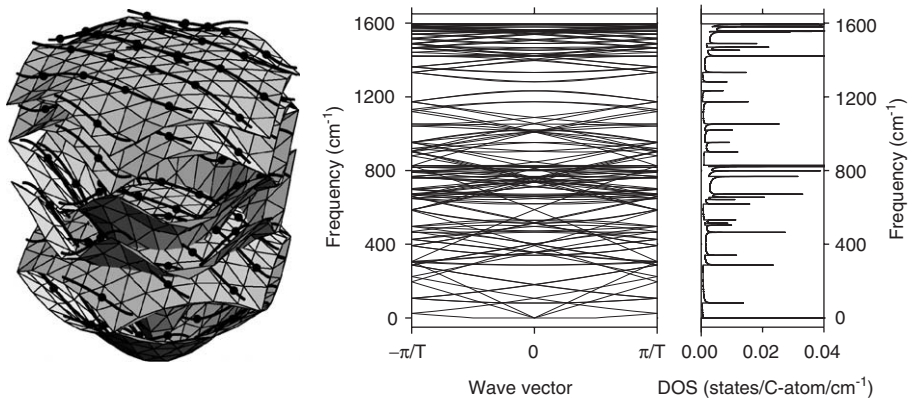

Fig. 14. (a) The phonon dispersion relations of the graphene layer in the first Brillouin zone calculated with the force constants fitted to the Raman scattering data for various graphitic materials. Solid curves show the cutting lines for the (4, 2) nanotube. Solid dots show the ends of the cutting lines in the 2-atom unit cell linear–helical representation. (b) Phonon modes for the (4, 2) nanotube obtained by zone-folding from (a). (c) Density of states for the phonon modes shown in (b). Spikes appear in the density of phonon states of the carbon nanotube, similar to the spikes (VHSs) appearing in the electronic DOS discussed in Section 5.

because of the three degrees of freedom per atom (see Fig. 14(a)). Superimposing the N cutting lines in the 2-atom linear–helical reciprocal structure of the nanotube on the six phonon frequency surfaces in the reciprocal space of the graphene layer yields $6N$ phonon branches for each carbon nanotube (see Fig. 14(b)), according to the zone-folding scheme as described in Section 2.4.2.

Group theory provides accurate information on both the number of phonons and the irreducible representations for the lattice modes $\mathscr{D}_{\text{lat. mod.}}$ that are obtained by taking the direct product of the irreducible representations for the atomic sites $\mathscr{D}^{\text{a.s.}}$ with that of the vector [8] ($\mathscr{D}_{\text{lat. mod.}} = \mathscr{D}^{\text{a.s.}} \otimes \mathscr{D}_{\text{vec.}}$). For $k = 0$ phonons in achiral tubes, the factor group is isomorphic to the D_{2nh} group, where $\mathscr{D}_{\text{vec}} = A_{2u} + E_{1u}$. The $\mathscr{D}^{\text{a.s.}}$ for zigzag SWNTs is [6]:

$$\mathscr{D}^{\text{a.s.}}_{\text{zigzag}} = A_{1g} + B_{2g} + A_{2u} + B_{1u} + \sum_{j=1}^{n-1}(E_{jg} + E_{ju}), \tag{38}$$

giving rise to the following irreducible representations for the lattice modes [6]:

$$\mathscr{D}^{\text{lat. mod.}}_{\text{zigzag}} = 2A_{1g} + A_{2g} + B_{1g} + 2B_{2g} + A_{1u} + 2A_{2u} + 2B_{1u} + B_{2u} + \sum_{j=1}^{n-1}(3E_{jg} + 3E_{ju}). \tag{39}$$

The phonon modes of carbon nanotubes can also be associated with the irreducible representations of the factor groups by applying the zone-folding scheme to the two-dimensional phonon dispersion relations of the graphene layer (see Figs. 14(a) and (b)), in a similar fashion as has been used to describe the electronic dispersion relations in Section 5. In such an analysis, the $6((N/2) - 1)$ pairs of phonon modes arising from the cutting lines with indices $\tilde{\mu}$ and $-\tilde{\mu}$, where $\tilde{\mu} = 1, \ldots, ((N/2) - 1)$, are expected to be doubly degenerate, while the phonon modes associated with cutting lines with indices $\tilde{\mu} = 0$ and $N/2$ are non-degenerate.

However, the zone-folding scheme in Fig. 14(a) neglects the curvature of the nanotube wall, as was already mentioned in Section 5. Meanwhile, the curvature couples the in-plane and out-of-plane phonon modes of the graphene layer to each other, especially affecting the low-frequency acoustic phonon modes. Among the three acoustic phonon modes of the graphene layer, only one of the two in-plane modes results in an acoustic phonon mode of the nanotube corresponding to the vibrational motion along the nanotube axis. The two other in-plane and out-of-plane acoustic phonon modes give rise to the twisting mode (TW, the vibrational motion in the circumferential direction of the nanotube) and to the radial breathing mode (RBM, the vibrational motion in the radial direction of the nanotube), correspondingly. The two related acoustic phonon modes of the nanotube (the vibrational motion in two orthogonal

directions perpendicular to the nanotube axis) can be constructed as linear combinations of the RBM and TW modes. The zone-folding scheme predicts zero frequencies for the A_{1g} (or A_1) perfectly symmetric RBM and TW phonon modes of the nanotube at the center of the Brillouin zone, since they arise from the zone folding of the acoustic phonon modes of the graphene layer. However, the curvature of the graphene layer affects the frequency of the RBM phonons resulting in their having non-zero frequencies. In fact, the frequency of the perfectly symmetric RBM is inversely proportional to the nanotube diameter, varying from around 100 to 250 cm^{-1} for typical nanotube diameters of 1–2 nm.

7. Selection rules for optical phenomena

In spite of the large number of electronic and phonon subbands in carbon nanotubes (see Figs. 10 and 14), very few of them participate in light absorption, Raman scattering, or infrared spectroscopy, because of symmetry restrictions. The selection rules governing the above mentioned processes are commonly derived from group theory. At the same time, the selection rules are closely related to the concept of cutting lines, and they can be easily obtained from the zone-folding procedure. In the present section, we focus on the selection rules for the electron–photon interaction in chiral and achiral carbon nanotubes in view of the space group theory developed in Section 3, but without considering the presence of excitons. Because of the importance of the excitonic effects in the optical properties of carbon nanotubes [35–37], we will discuss excitonic effects from the standpoint of group theory in Section 8.

7.1. Selection rules for optical absorption from space group theory

The electromagnetic interaction giving rise to electric dipole transitions is

$$H'_{\mathrm{em}} = -\frac{e}{2mc}\vec{p}\cdot\vec{A}, \tag{40}$$

in which $\vec{p}$ is the momentum of the electron and $\vec{A}$ is the vector potential of an external electromagnetic field. The momentum operator is part of the physical system under consideration, while the vector $\vec{A}$ acts like the *bath* or *reservoir* in a thermodynamic sense. Thus, $\vec{p}$ acts like an operator with respect to Schrödinger's equation, but $\vec{A}$ does not. Therefore, H'_{em} for the electromagnetic interaction transforms like a vector in the context of the group of Schrödinger's equation for the unperturbed system $H_0\psi = E\psi$. It is then clear that the Hamiltonian describing the electron–photon interaction will transform as a vector in the direction of the polarization of the light. Therefore for light polarized along the nanotube axis, the electron–photon interaction at $k=0$ will transform as the vector z. For achiral (chiral) nanotubes, the vector z transforms as the A_{2u} (A_2) irreducible representation of the factor group at $k=0$ which is isomorphic to the D_{2nh} (D_N) point group (see Table 3(1)). To obtain the selection rules for the optical absorption by the nanotube, it is necessary to take a direct product between the initial representation and the representation of the electron–photon interaction. It can be seen that the electronic energy bands that are in the energy range of the optical absorption have $E_{\tilde{\mu}}$ symmetries. Therefore, since the direct product leads to $A_2 \otimes E_{\tilde{\mu}} = E_{\tilde{\mu}}$, the selection rules require that $\delta\tilde{\mu} = 0$ for light polarized along the tube axis. The effect of an operation with A_{2u} symmetry is to reverse the parity of the $E_{\tilde{\mu}}$ representation, and therefore, for achiral nanotubes, the state with $E_{\tilde{\mu}u}$ symmetry is coupled to a state with $E_{\tilde{\mu}g}$ symmetry and vice-versa by the electromagnetic interaction.

In the case of light polarized perpendicular to the nanotube axis, the electron–photon interaction transforms as the vectors x and y, which correspond to the E_1 representation of the factor group of chiral nanotubes and the E_{1u} representation for achiral carbon nanotubes. The selection rules then require $\delta\tilde{\mu} = \pm 1$, since $E_1 \otimes E_{\tilde{\mu}} = E_{\tilde{\mu}\pm 1}$.

7.2. Selection rules for Raman and infrared spectroscopy from group theory

The optical activity of phonons in a first-order Raman or infrared scattering process is easily obtained from the basis functions related to the irreducible representations of the lattice modes. The Raman-active modes are those transforming like symmetric combinations of quadratic functions (xx, yy, zz, xy, yz, zx), and the infrared-active modes are those transforming like vectors (x, y, z).

The list of Raman and infrared-active modes are given below [6,7]:

$$\mathscr{D}^{\text{Raman}}_{\text{zigzag}} = 2A_{1g} + 3E_{1g} + 3E_{2g} \rightarrow 8 \text{ modes}; \tag{41}$$

$$\mathscr{D}^{\text{infrared}}_{\text{zigzag}} = A_{2u} + 2E_{1u} \rightarrow 3 \text{ modes}; \tag{42}$$

$$\mathscr{D}^{\text{Raman}}_{\text{armchair}} = 2A_{1g} + 2E_{1g} + 4E_{2g} \rightarrow 8 \text{ modes}; \tag{43}$$

$$\mathscr{D}^{\text{infrared}}_{\text{armchair}} = 3E_{1u} \rightarrow 3 \text{ modes}; \tag{44}$$

$$\mathscr{D}^{\text{Raman}}_{\text{chiral}} = 3A_1 + 5E_1 + 6E_2 \rightarrow 14 \text{ modes}; \tag{45}$$

$$\mathscr{D}^{\text{infrared}}_{\text{chiral}} = A_2 + 5E_1 \rightarrow 6 \text{ modes}. \tag{46}$$

A more detailed analysis of the Raman active modes for chiral and achiral nanotubes is provided in Ref. [7].

To illustrate the usage of the selection rules introduced by the electron–photon and electron–phonon interaction processes, we consider the first-order resonance Raman scattering process in carbon nanotubes [38,39]. The first-order Raman scattering process involves the following steps: creation of an electron–hole pair, scattering by a phonon, and light emission by an electron–hole recombination process [38,39]. The Raman signal is greatly enhanced when the electron scatters between VHSs in the valence and conduction band DOS, so that we can consider only the transitions between the two VHSs in the DOS as a first approximation. By utilizing the selection rules introduced above, we come up with the following five cases for the allowed first-order resonance Raman scattering processes in chiral SWNTs between the electronic energy VHSs in the valence and conduction bands denoted by $\mathbb{E}^{(v)}_{\mu}$ and $\mathbb{E}^{(c)}_{\mu'}$ for a general k point in the Brillouin zone [40]:

$$\begin{aligned}
&\text{(I)}\ \mathbb{E}^{(v)}_{\tilde{\mu}} \xrightarrow{Z} \mathbb{E}^{(c)}_{\tilde{\mu}} \xrightarrow{A} \mathbb{E}^{(c)}_{\tilde{\mu}} \xrightarrow{Z} \mathbb{E}^{(v)}_{\tilde{\mu}},\\
&\text{(II)}\ \mathbb{E}^{(v)}_{\tilde{\mu}} \xrightarrow{X} \mathbb{E}^{(c)}_{\tilde{\mu}\pm1} \xrightarrow{A} \mathbb{E}^{(c)}_{\tilde{\mu}\pm1} \xrightarrow{X} \mathbb{E}^{(v)}_{\tilde{\mu}},\\
&\text{(III)}\ \mathbb{E}^{(v)}_{\tilde{\mu}} \xrightarrow{Z} \mathbb{E}^{(c)}_{\tilde{\mu}} \xrightarrow{\mathbb{E}_1} \mathbb{E}^{(c)}_{\tilde{\mu}\pm1} \xrightarrow{X} \mathbb{E}^{(v)}_{\tilde{\mu}},\\
&\text{(IV)}\ \mathbb{E}^{(v)}_{\tilde{\mu}} \xrightarrow{X} \mathbb{E}^{(c)}_{\tilde{\mu}\pm1} \xrightarrow{\mathbb{E}_1} \mathbb{E}^{(c)}_{\tilde{\mu}} \xrightarrow{Z} \mathbb{E}^{(v)}_{\tilde{\mu}},\\
&\text{(V)}\ \mathbb{E}^{(v)}_{\tilde{\mu}} \xrightarrow{X} \mathbb{E}^{(c)}_{\tilde{\mu}\pm1} \xrightarrow{\mathbb{E}_2} \mathbb{E}^{(c)}_{\tilde{\mu}\mp1} \xrightarrow{X} \mathbb{E}^{(v)}_{\tilde{\mu}},
\end{aligned} \tag{47}$$

where A, E_1, and E_2 denote the symmetries of the phonon modes at $k=0$, which are associated with the $\tilde{\mu}=0$, $\tilde{\mu}=\pm1$, and $\tilde{\mu}=\pm2$ cutting lines, respectively. The XZ plane is parallel to the substrate on which the nanotubes lie, the Z axis is directed along the nanotube axis, and the Y axis is directed along the light propagation direction, so that Z and X in Eq. (47) stand for the light polarized parallel and perpendicular to the nanotube axis, respectively.

The five processes of Eq. (47) result in different polarization configurations for different phonon modes, ZZ and XX for A; ZX and XZ for E_1; and XX for E_2, in perfect agreement with the basis functions predicted by group theory. Also, Eq. (47) predicts *different* resonance conditions for *different* phonon modes. The A and E_1 modes can be observed in resonance for the $\mathbb{E}^{(v)}_{\tilde{\mu}} \rightarrow \mathbb{E}^{(c)}_{\tilde{\mu}}$ and the $\mathbb{E}^{(v)}_{\tilde{\mu}} \rightarrow \mathbb{E}^{(c)}_{\tilde{\mu}\pm1}$ processes, corresponding to E_{ii} and E_{ij} $(j \neq i)$ transitions, respectively, the E_2 modes can only be observed in resonance for the $\mathbb{E}^{(v)}_{\tilde{\mu}} \rightarrow \mathbb{E}^{(c)}_{\tilde{\mu}\pm1}$ process. Experimentally observed Raman scattering spectra follow the predicted polarization configurations and resonance conditions [40,41].

7.3. Selection rules for double resonance Raman processes

As explained in Section 7.2, only a few of the phonon branches in carbon nanotubes are Raman active. However, many peaks are observed experimentally in the carbon nanotube Raman spectra which are present due to a process known as double resonance Raman scattering (DRRS) [42,43]. In this process, the electron in the valence band is excited to a conduction band state, from which it is scattered by either a phonon or a lattice defect into another electronic state

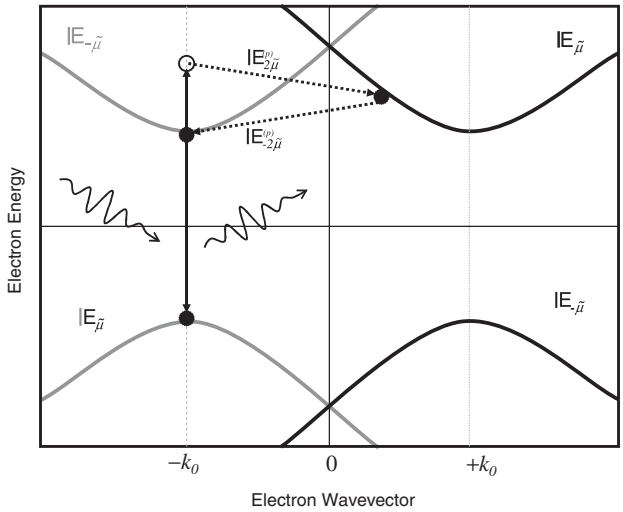

Fig. 15. Diagram showing a possible double resonance process for chiral nanotubes. The electron is excited to the $\mathbb{E}_{-\tilde{\mu}}$ electronic band by a photon, scattered to the $\mathbb{E}_{\tilde{\mu}}$ electronic band by a phonon with $\mathbb{E}_{2\tilde{\mu}}$ symmetry and then scattered back to the $E_{-\tilde{\mu}}$ electronic band, for which it can recombine optically, emitting a photon [42].

and then scattered back to the same initial state in the conduction band (in the case of light polarized parallel to the nanotube axis) by either another phonon or by a lattice defect. The electron can then emit a photon and recombine with the photo-induced hole. In the DRRS process it is necessary that two out of the three states in the conduction band which are visited by the electron are real electronic states, giving rise to a resonance process. If that is the case, the Raman cross section is strongly enhanced, resulting in an efficient Raman process. The selection rules for the optical excitation and emission in parallel polarization determine that the initial and final k value of the electron should be the same, in order to guarantee vertical electronic transitions, which will be dipole allowed (see Section 7.1). Therefore, the electronic states which are visited in the conduction band are determined by the energy difference between the electronic bands, by the conservation of linear momentum, and by obeying the relevant selection rules. In the vicinity of the Fermi energy, the electronic states of a general chiral nanotube will have $E_{\pm\tilde{\mu}}$ symmetry. Thus, for a transition to occur between the electron in a state $E_{\tilde{\mu}_1}$ and a state $E_{\tilde{\mu}_2}$ it is necessary that the phonon which couples the two states has $E_{\tilde{\mu}_2-\tilde{\mu}_1}$ symmetry. In Fig. 15, we show a possible double resonance process between two electronic bands with symmetries $E_{-\tilde{\mu}}$ and $E_{\tilde{\mu}}$, which have the same eigenenergies for wavevectors k and $-k$. The phonon which couples these two bands has either $E_{2\tilde{\mu}}$ or $E_{-2\tilde{\mu}}$ symmetry, and the superscript (p) is used in Fig. 15 to denote phonon.

7.4. Selection rules from zone folding

In the previous section the selection rules for the quantum numbers were obtained by symmetry considerations. It is interesting to discuss how equivalent selection rules can be derived considering momentum conservation in the unfolded two-dimensional graphene-sheet, considering the concepts of cutting lines.

The optical transition in the nanotube is vertical within the 1D Brillouin zone, i.e., the electronic wave vector along the nanotube axis (along the $\vec{K}_2$ vector in the unfolded 2D Brillouin zone) does not change. In contrast to the case of the graphene layer, the polarization vector can be either parallel or perpendicular to the nanotube axis for light propagating perpendicular to the substrate on which the nanotubes lie. The dipole selection rules tell us that the optical transition in the nanotube conserves the electronic subband index (the cutting line index $\tilde{\mu}$) for light polarized parallel to the nanotube axis (see Section 7.1). Conservation of both the 1D wave vector and the subband index implies conservation of the 2D wave vector in the Brillouin zone of the graphene layer (unfolded Brillouin zone of the nanotube).

As an example, we plot in Fig. 16 the schematic band diagram of the nanotube in the unfolded 2D Brillouin zone. If an electron in the valence subband V2U of Fig. 16 (see the parabolic curve in Fig. 16 labeled V2U) absorbs a photon, the electron goes vertically to the conduction subband C2L. If the electron starts from the VHS in the valence subband

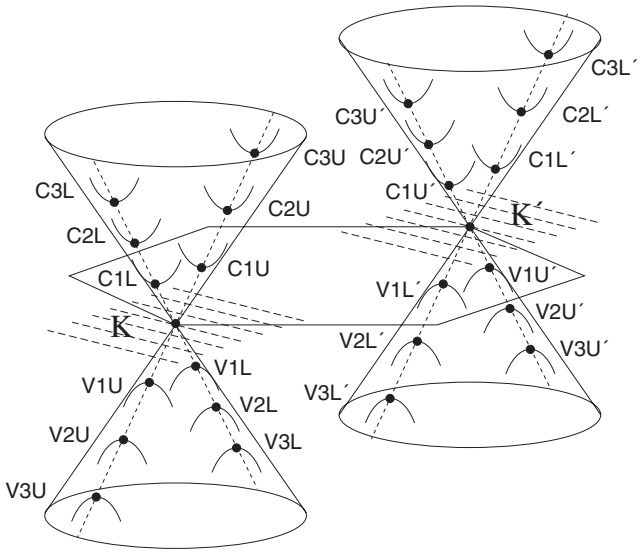

Fig. 16. The electronic subbands for zigzag metallic nanotubes in the vicinity of the K and K' (near the Fermi energy) points in the first Brillouin zone. The VHSs are labeled by three symbols, the first denotes valence or conduction band (C/V), the second denotes the VHS index counted away from the Fermi energy or the cutting line index counted away from the K and K' points, and the third denotes the lower and upper energy components (L/U) due to the trigonal warping effect that splits the energy of the VHSs for metallic SWNTs [44].

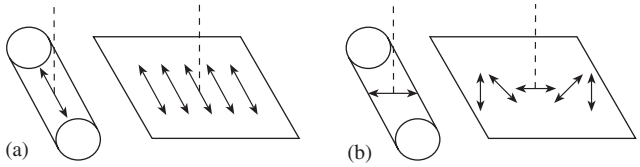

Fig. 17. Light polarization (a) parallel and (b) perpendicular to the nanotube axis, shown for both a rolled-up SWNT (left), and a SWNT unrolled into the graphene layer (right). The arrows show the light polarization vector, and the dashed lines show the light propagation direction [14].

V2U (see the solid dot on the subband V2U in Fig. 16), this electron goes to the VHS in the conduction subband C2L, and the optical absorption is enhanced substantially because of the extremely high DOS at the VHSs in the valence and conduction subbands, V2U and C2L.

If an electron in the valence subband V2U in Fig. 16 absorbs a photon polarized perpendicular to the nanotube axis (i.e., polarized along the $\vec{K}_1$ vector), it can scatter to one of the two conduction subbands, either C1L or C3L. This implies a different set of VHSs in the JDOS for perpendicular polarization, $E_{\tilde{\mu},\tilde{\mu}\pm1}$.

While the optical transition is vertical for the light polarized parallel to the nanotube axis, it involves a wave vector change of $\pm\vec{K}_1$ (the distance between two adjacent cutting lines) for the perpendicular polarization. This wave vector change can be easily understood by considering an unrolled nanotube, as shown in Fig. 17. When the nanotube is unrolled into the graphene layer, the light polarized parallel to the nanotube axis transforms into light polarized parallel to the graphene layer, as shown in Fig. 17(a), resulting in a vertical interband optical transition in the unfolded 2D Brillouin zone, which is equivalent to the optical transition within the same subband $\tilde{\mu}$ in the folded 1D Brillouin zone of the nanotube, as is predicted by the dipole selection rules.

However, perpendicular polarization in nanotubes becomes transformed into the in-plane and out-of-plane polarizations in the unfolded graphene layer, periodically modulated along the direction of the $\vec{K}_1$ vector with the period πd_t (nanotube circumference), as shown in Fig. 17(b) [14]. The optical transitions induced by the out-of-plane polarization are expected to be much weaker compared to those induced by the in-plane polarization and are usually ignored, because of the much stronger in-plane interaction in the graphene layer [45]. This implies that the light polarization in the unrolled nanotube shown in Fig. 17(b) can be considered, as a first approximation, to be parallel to the graphene

layer, with an additional phase factor describing oscillations of the in-plane polarization component, arising from the rotation of the polarization vector. The phase factor is given by $\cos(\vec{k}\cdot\vec{r})$ where the wave vector $\vec{k}$ has the direction of $\vec{K}_1$ and a magnitude of $2\pi/(\pi d_t) = 2/d_t$, i.e., $\vec{k} = \vec{K}_1$. By assuming wave vector conservation in the unfolded 2D Brillouin zone for the optical transition process, we come up with the selection rules $\vec{k}_c = \vec{k}_v \pm \vec{K}_1$ for light absorption and $\vec{k}_v = \vec{k}_c \pm \vec{K}_1$ for light emission, which correspond to an electronic transition to the adjacent cutting line in the unfolded 2D Brillouin zone, or the electronic transition to the adjacent subband in the 1D Brillouin zone of the nanotube. It is interesting to note that the photon wave vector $\pm\vec{K}_1$ in the unrolled graphene layer is much larger in magnitude than the photon wave vector κ in free space, $K_1 = 2/d_t \gg \kappa = 2\pi/\lambda$, because the nanotube diameter d_t is much smaller than the optical wave length λ. Therefore, an optical photon in the unrolled graphene layer can be considered as an X-ray photon with respect to spatial considerations, yet the photon energy does not change when the nanotube is unrolled into the graphene layer. Such a "pseudo X-ray" photon is a source of breaking the optical selection rules in the case of perpendicular polarization.

The selection rules for the scattering of electrons by phonons can also be obtained by momentum conservation in 2D graphite. Two cutting lines belonging to the irreducible representations E_μ and $E_{\mu'}$ are separated from each other in the 2D Brillouin zone by $\vec{k} - \vec{k}' = (\tilde{\mu} - \tilde{\mu}')2\pi/d_t$, and this is the momentum that the phonon should transfer as a result of the transition. As explained in Section 6, the symmetry of the phonon with such a momentum can be obtained by rolling up the 2D graphene layer and this will yield a phonon with $E_{\tilde{\mu}-\tilde{\mu}'}$ symmetry.

8. Excitons in carbon nanotubes

Due to the strong spatial confinement of carriers in 1D materials, the electron–hole Coulomb interaction is strong. Therefore, it has been predicted that excitonic effects should dominate the optical transitions in semiconducting carbon nanotubes [35,46,47]. This fact has been confirmed experimentally by comparing the energies for 1-photon and 2-photon excitations, which excite different excitonic states [36,37]. Rigorously, excitons originate from a many-body description of electron–electron and electron–hole interactions. However, to obtain the symmetry of the excitonic states, it is only necessary to have the correct symmetry for the Hamiltonian. Thus, although a detailed mathematical analysis of the many-body interactions is necessary to obtain the quantitative information, such as accurate values for energy levels, eigenfunctions, matrix elements, transition probabilities, etc., the proper form for the electron–hole interaction is sufficient to obtain the correct symmetry properties for excitons in carbon nanotubes.

Also, for a full description of excitons in carbon nanotubes, it is necessary to consider the exchange of the electrons and holes involved in the formation of the excitonic states. The symmetry properties of the singlet and triplet excitonic states formed by the combinations of electrons and holes when considering the presence of exchange interaction can be obtained using the formalism of double groups [8]. Although the exchange interaction is known to be weak [48], implying a small splitting between the singlet and the triplet states, the selection rules for creating and annihilating triplet states is somewhat different from that of singlet states. Therefore, to fully understand the exciton dynamics from the point of view of symmetry, it is necessary to have a complete study of the electronic properties of carbon nanotubes within the formalism of double groups. However, the study of the formalism of double groups applied to nanotubes is not available in the literature. Therefore, we will focus the present work on the symmetry properties of singlet exciton states, which can be analyzed using the space group theory developed in Section 3, without taking the exchange between the electrons and holes into consideration.

8.1. The exciton symmetries

The exciton wavefunction can be written as a linear combination of products of conduction (electron) and valence (hole) eigenstates as

$$\psi(\vec{r}_\mathrm{e}, \vec{r}_\mathrm{h}) = \sum_{v,c} A_{vc}\phi_c(\vec{r}_\mathrm{e})\phi_v^*(\vec{r}_\mathrm{h}), \tag{48}$$

where v and c stand for valence- and conduction-band states, respectively. To obtain an accurate solution for the excitonic eigenfunctions (the A_{vc} coefficients) and eigenenergies, it is necessary to solve the Bethe–Salpeter equation [47,49], which includes many-body interactions and considers the mixing by the Coulomb interaction of electron and hole states with all the different wavevectors of all the different bands. The Coulomb interaction depends only on the

relative distance between the electron and the hole, and thus the many-body Hamiltonian is invariant under the symmetry operations of the nanotube. Each excitonic eigenstate will then transform as one of the irreducible representations of the space group of the nanotube. In general the electron–hole interaction will mix states with all wavevectors and all bands, but for moderately small-diameter nanotubes ($d_t < 1.5$ nm), the separation between singularities in the single-particle JDOS (joint density of states) is fairly large and it is reasonable to consider, as a first approximation, that only the electronic bands contributing to a given singularity will mix to form the excitonic states [47]. Within this approximation, it is possible to employ the usual effective-mass and envelope-function approximations (EMA) to obtain the exciton eigenfunctions [50]:

$$\psi^{\mathrm{EMA}}(\vec{r}_{\mathrm{e}}, \vec{r}_{\mathrm{h}}) = \sum_{v,c}{}' B_{eh}\phi_e(\vec{r}_{\mathrm{e}})\phi_h^*(\vec{r}_{\mathrm{h}})F_v(z_{\mathrm{e}} - z_{\mathrm{h}}). \tag{49}$$

The prime in the summation indicates that only the electron and hole states associated with the JDOS singularity are included. It is important to emphasize that the approximate wavefuntions ψ^{EMA} have the same symmetries as the full wavefunctions ψ. The envelope function $F_v(z_{\mathrm{e}} - z_{\mathrm{h}})$ provides an ad-hoc localization of the exciton in the relative coordinate $z_{\mathrm{e}} - z_{\mathrm{h}}$ along the axis and v labels the levels in the 1D hydrogenic series [51]. The envelope functions will be either even ($v = 0, 2, 4\ldots$) or odd ($v = 1, 3, 5\ldots$) upon $z \to -z$ operations. The use of such "hydrogenic" envelope-functions serves merely as a physically grounded guess to the ordering in which the different exciton states might appear.

From Eq. (49), we can see that the irreducible representation of the excitonic state $\mathscr{D}(\psi^{\mathrm{EMA}})$ will be given by the direct product between the irreducible representation of the envelope function and the irreducible representation of the electron and hole states at the band-edges [50]:

$$\mathscr{D}(\psi^{\mathrm{EMA}}) = \mathscr{D}(\phi_e) \otimes \mathscr{D}(\phi_h) \otimes \mathscr{D}(F_v), \tag{50}$$

where $\mathscr{D}(\phi_e)$, $\mathscr{D}(\phi_h)$ and $\mathscr{D}(F_v)$ are the irreducible representations of the electron state, hole state and envelope function, respectively.

To study the exciton symmetries in chiral, zigzag and armchair tubes we now apply Eq. (50) considering that the group of the wavevector for the exciton can be obtained from the excitonic center of mass wavevector $K = k_{\mathrm{e}} + k_h$.

8.1.1. Chiral nanotubes

Let us now consider the first optical transition (E_{11}) in chiral nanotubes. As shown in Fig. 18(a), the minimum energy gap occurs at two inequivalent wavevectors $k = \pm k_0$. The electronic states associated with a band $\tilde{\mu}$ and a wavevector k away from the zone center ($k \neq 0$) transform as the 1D representations $\mathbb{E}_{\tilde{\mu}}(k)$ of the C_N point group (see Section 5). Therefore, the electron and hole in states the VHS will, respectively, belong to the $\mathbb{E}_{\pm\tilde{\mu}}(\pm k_0)$ and $\mathbb{E}_{\mp\tilde{\mu}}(\mp k_0)$ irreducible representations. Both the electron and hole states are degenerate in energy at $k = k_0$ and $k = -k_0$ due to time reversal symmetry, and thus it is expected that the Coulomb interaction will strongly mix these two electrons and two hole states, resulting in four exciton states. In the case of the lowest-energy envelope function ($v = 0$), which is even and transforms as the totally symmetric representation $A_1(0)$, Eq. (50), can be written for each possible electron–hole pair:

$$\begin{cases} \mathbb{E}_{\tilde{\mu}}(k_0) \otimes \mathbb{E}_{-\tilde{\mu}}(-k_0) \otimes A_1(0), \\ \mathbb{E}_{-\tilde{\mu}}(-k_0) \otimes \mathbb{E}_{\tilde{\mu}}(k_0) \otimes A_1(0), \\ \mathbb{E}_{\tilde{\mu}}(k_0) \otimes \mathbb{E}_{\tilde{\mu}}(k_0) \otimes A_1(0), \\ \mathbb{E}_{-\tilde{\mu}}(-k_0) \otimes \mathbb{E}_{-\tilde{\mu}}(-k_0) \otimes A_1(0). \end{cases} \tag{51}$$

It should be noted that the representations of the electron states, hole states and the envelope function are, in general, associated with different wavevectors ($\pm k_0$ for electron and hole states and 0 for the envelope function), and thus belong to different point groups. Also, the final excitonic states will be associated with another different wavevector for the center of mass $K = k_{\mathrm{e}} + k_{\mathrm{h}}$. In order to obtain the results of the direct products between representations in different point groups, it is necessary to make use of the compatibility between the C_N and D_N point groups (see Table 5).

The direct product between electrons and holes with opposite quantum numbers $(k_{\mathrm{e}}, \tilde{\mu}_{\mathrm{e}}) = (-k_{\mathrm{h}}, -\tilde{\mu}_{\mathrm{h}}) = \pm(k_0, \tilde{\mu})$ (first two lines in Eq. (51)) will result in two exciton states with quantum numbers $(K, \tilde{\mu}') = (0, 0)$ and which will transform as the A irreducible representation of the C_N point group. However, the group of the wavevector $K = 0$ is the

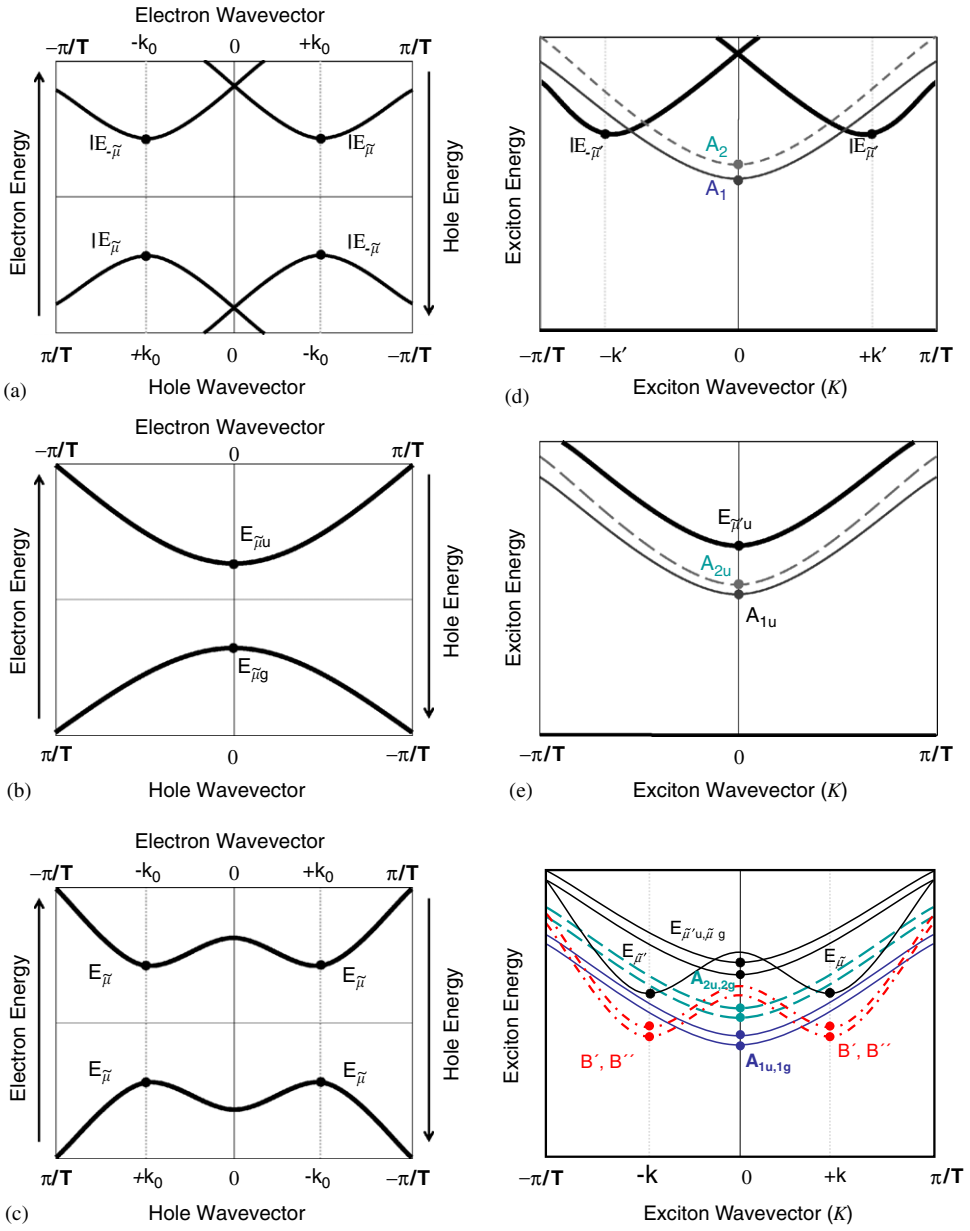

Fig. 18. Diagrams for the electronic bands and symmetries for: (a) chiral (n, m); (b) zigzag $(n, 0)$; and (c) armchair (n, n) nanotubes and for their respective excitonic bands (d), (e) and (f). The electron, hole and exciton states at the band edges are indicated by a solid circle and labeled according to their irreducible representations. Different line types and colors in this figure are related to bands with different symmetries. Thick (black) solid lines correspond to the $E_{\tilde{\mu}'}$ representation, the blue (thin) solid lines correspond to A_1 excitons while the cyan (thin) dashed lines correspond to the A_2 excitonic states. In the case of achiral nanotubes, we also have inversion and mirror plane symmetries. For a better visualization, the bands with different parities under the inversion and mirror plane symmetry operations were grouped together and appear with the same line color and pattern. In the case of armchair nanotubes, the bands which transform as the B' and B'' representations are shown using a red dot-dash pattern. The electronic and excitonic band structures shown here are only pictorial. Group theory does not order the values for the eigenenergies and energy dispersions.

D_N point group, and thus one of these states will transform as the A_1 representation and the other as the A_2 representation of the D_N point group. These states correspond, respectively, to states even and odd under the C_2 rotation. The direct product with the $A_1(0)$ irreducible representations of the envelope function will leave both irreducible representations unchanged.

The mixing between electron and hole states with the same quantum numbers $(k_e, \tilde{\mu}_e) = (k_h, \tilde{\mu}_h) = \pm(k_0, \tilde{\mu})$ (two last lines in Eq. (51)) will result in two exciton states with quantum numbers $\pm(2k_0, 2\tilde{\mu})$. We now need to observe that the group of the wavevector k is only defined for values of k within the 1st Brillouin zone and $\tilde{\mu}$ between $-N/2+1$ and $N/2$. If $2k_0$ crosses the boundary of the 1st Brillouin zone, the linear and quasi-angular quantum numbers of the excitonic states will be corrected to

$$\begin{cases} k' = 2k_0 \mp 2\pi/T, \\ \tilde{\mu}' = 2\tilde{\mu} \pm M. \end{cases} \tag{52}$$

Here, we use the value M, which was defined in Section 2.4.2. The $\mp$ corresponds to the cases where $2k_0 > \pi/T$, while the $\pm$ sign corresponds to cases where $2k_0 < -\pi/T$. If the quasi-angular momentum $|\tilde{\mu}'|$ is larger than $N/2$ it will also have to be corrected to

$$\tilde{\mu}' = \tilde{\mu} \mp N, \tag{53}$$

and here the "−" and "+" signs correspond to $\tilde{\mu}' > N/2$ and $\tilde{\mu}' < -N/2$, respectively. These corrections for k' and $\tilde{\mu}'$ for the excitonic states follow from the rules of translations in reciprocal space for the linear–helical approach (see Section 2.4.2). We see that the direct product between the electron and hole states with the same quantum numbers will lead to excitons with symmetries $\mathbb{E}_{\pm\tilde{\mu}'}(\pm k')$, since, in general, the group of the wavevector $k' = 2k_0$ is the C_N point group (except in the specific cases of $k_0 = 0$ and $\pi/(2T)$). Again, we note that the direct product with the envelope function leaves the irreducible representations unchanged.

For a better understanding on how to obtain the correct representations for the excitonic states we will follow the example of correctly representing the (8, 2) nanotube, which is metallic, but still can have excitonic states. For this particular nanotube, the value of N is 28 and the lowest energy electronic transition occurs between electron and hole states with $\tilde{\mu} = \pm 7$. Also, the states at the electronic band edges for this nanotube occur at $k_0 \sim \pm 2\pi/3T$. Following Eq. (51), there will be two exciton states at $K = 0$, one with A_1 symmetry and one with A_2 symmetry, and two excitons with $\mathbb{E}$ symmetry with a band edge at k'. The quantum numbers for the $\mathbb{E}$ symmetry exciton states would be $2\tilde{\mu} = \pm 14$ and $2k_0 \sim \pm 4\pi/3T$. The irreducible representations for these excitons can be obtained by first translating the linear wavevector $2k_0$ back to the first Brillouin zone, which leads to $k' \sim \pm(4\pi/3T - 2\pi/T) = \mp 2\pi/3T$ and $\tilde{\mu}' = \pm(2\tilde{\mu} + 10) = \pm 24$, since $M = 10$ for the (8, 2) nanotube. Since $|\tilde{\mu}'| = 24 > N/2$, we need to find the correct label $\tilde{\mu}'$ for the irreducible representation by subtracting $N = 28$ from 24, which results in $\tilde{\mu}' = \mp 4$. Therefore, we conclude that the excitons formed from the 1st VHS in the (6, 5) nanotube will have symmetries $A_1(0)$, $A_2(0)$, $\mathbb{E}_{-4}(-k_0)$ and $\mathbb{E}_4(k_0)$, where we have considered that $k' \sim 2\pi/3T = k_0$.

The symmetry of the exciton states away from the band edge can be obtained by applying the compatibility relations between the D_N and C_N point groups. The excitonic bands which have a band edge at $K = 0$ will both have symmetry A away from the center of the Brillouin zone, while the excitonic bands which have symmetries $\mathbb{E}_{\pm\tilde{\mu}'}$ at $K = \pm k'$ will be brought together at the zone center ($K = 0$) to form a doubly degenerate 2-dimensional representation $E_{2|\tilde{\mu}|}(0)$ of the D_N point group. Therefore, group theory shows that the lowest energy set of excitons is composed of four exciton bands, shown schematically in Fig. 18(d).

Let us now consider higher-energy exciton states in chiral tubes. Those can be obtained, for instance, by considering the same VHS in the JDOS and higher values of v. For v even, the resulting decomposition is the same, since the envelope function also has A_1 symmetry. For odd values of v, the envelope function will transform as A_2, but this will only exchange the A_1 and A_2 symmetry excitons, and will leave $\mathbb{E}$ symmetry excitons unchanged. The result is still the same if one considers now higher-energy exciton states derived from higher singularities in the JDOS (for instance, the so-called E_{22} transitions). Therefore, we can write an equation which describes the symmetries of all exciton states associated with E_{ii} transitions in chiral nanotubes as

$$(\mathbb{E}_{\tilde{\mu}}(k_0) + \mathbb{E}_{-\tilde{\mu}}(-k_0)) \otimes (\mathbb{E}_{-\tilde{\mu}}(-k_0) + \mathbb{E}_{\tilde{\mu}}(k_0)) \otimes A_{1,2}(0) = A_1(0) + A_2(0) + \mathbb{E}_{\tilde{\mu}'}(k') + \mathbb{E}_{-\tilde{\mu}'}(-k'),$$

where A_1 and A_2 are related to v even and odd envelope functions, respectively, and k' and $\tilde{\mu}'$ are the quantum numbers associated with the exciton linear and quasi-angular momenta, as obtained above. It should be mentioned that the values of $\tilde{\mu}$ and k_0 will be different for each nanotube and also for each E_{ii} transition.

The situation differs for the so-called E_{ij} transitions, with $i \neq j$. Specifically, the transitions for which the quasi-angular momentum of the valence and conduction bands differ by ± 1 are more relevant experimentally because,

as we shall see later in Section 8.2, they may be observed for perpendicular polarization. Therefore, we focus on that particular case and Eq. (50) now can be written as

$$(\mathbb{E}_{\tilde{\mu}}(k_0) + \mathbb{E}_{-\tilde{\mu}}(-k_0)) \otimes \left(\mathbb{E}_{-(\tilde{\mu}\pm1)}(-k_0') + \mathbb{E}_{\tilde{\mu}\pm1}(k_0')\right) \otimes A_{1,2}(0) = \mathbb{E}_{\pm1}(k') + (\mathbb{E}_{\tilde{\mu}'}(k') + \mathbb{E}_{-\tilde{\mu}'}(k'')),$$

where $A_1(0)$ and $A_2(0)$ are the irreducible representations of the envelope functions for v even and odd, respectively. It is important to note that for a general chiral nanotube, the valence and conduction band extrema occur at different $k = k_0$ and k_0' points, leading to non-zero exciton wavevectors k' and k'' for the all four exciton states.

8.1.2. Zigzag nanotubes

For zigzag nanotubes, the VHSs for the electronic bands associated with all E_{ii} transitions occur at $k_0 = 0$, and the electronic valence and conduction bands transform as either the $E_{\tilde{\mu}g}$ or the $E_{\tilde{\mu}u}$ irreducible representations of the D_{2nh} group. In contrast to chiral nanotubes, these irreducible representations for the electron and hole states are 2D, and thus correspond to degenerate states due to the inversion center symmetry. Although there is only one band edge in the 1D Brillouin zone, there are two electron and two hole states, which leads to four excitonic states. The symmetries of the excitonic states can be obtained form the direct product:

$$E_{\tilde{\mu}g}(0) \otimes E_{\tilde{\mu}u}(0) \otimes A_{1g}(0) = A_{1u}(0) + A_{2u}(0) + E_{\tilde{\mu}'u}(0) \tag{54}$$

for v even and

$$E_{\tilde{\mu}g}(0) \otimes E_{\tilde{\mu}u}(0) \otimes A_{2u}(0) = A_{2g}(0) + A_{1g}(0) + E_{\tilde{\mu}'g}(0) \tag{55}$$

for v odd.

The corresponding band structure for $v = 0$ (lowest exciton states) is shown in Fig. 18(e). It is interesting to note that, in this case, all four excitonic states have their band edges at the Γ point ($K = 0$). The symmetries of the excitonic states away from the Γ point for zigzag nanotubes can be obtained directly from the compatibility relations between the D_{2nh} and the C_{2nv} point groups. (See Table 6.)

For E_{ij} transitions with $i \neq j$ and quasi-angular momentum differing by ±1 in zigzag tubes, the situation is slightly more complicated because valence and conduction bands can have either the same or opposite parity under inversion. For example, the valence (conduction) bands of the (10, 0) tube, transform as $E_{7g}(E_{7u})$, $E_{6g}(E_{6u})$ and $E_{8u}(E_{8g})$ (listed in order of proximity to the gap). Therefore, transitions connecting $\tilde{\mu} = 6$ and 7 are between states of different parities, whereas transitions connecting $\tilde{\mu} = 7$ and 8 are between states of the same parity. Therefore, we need to consider the following cases:

$$E_{\tilde{\mu}\pi}(0) \otimes E_{(\tilde{\mu}\pm1)\pi}(0) \otimes A_{1g,2u}(0) = E_{\tilde{\mu}'g,u} + E_{1g,u}, \tag{56}$$

for valence and conduction states of the same parity, and:

$$E_{\tilde{\mu}\pi}(0) \otimes E_{(\tilde{\mu}\pm1)\bar{\pi}}(0) \otimes A_{1g,2u}(0) = E_{\tilde{\mu}'u,g} + E_{1u,g}, \tag{57}$$

for valence and conduction states of opposite parity. The envelope function label $1g$ or $2u$ correspond to v even or odd, respectively.

8.1.3. Armchair nanotubes

The optical transitions in armchair tubes are also excitonic, despite the metallic character of these tubes, because of symmetry gap effects [47]. As shown in Fig. 18(c), the E_{ii}-derived excitons will be formed by two electron and hole states each with symmetry $E_{\tilde{\mu}}$ and at the band edges at $k = \pm k_0$, where $k_0 \approx 2\pi/3a$ for the lowest electronic transition. Each of the bands is doubly degenerate, and therefore the Coulomb interaction is going to mix four different electron states with four different hole states which should result in 16 excitonic states. The symmetries of these excitons can be obtained using Eq. (50) and will result in

$$\begin{aligned}(E_{\tilde{\mu}}(k_0) + E_{\tilde{\mu}}(-k_0)) \otimes (E_{\tilde{\mu}}(k_0) + E_{\tilde{\mu}}(-k_0)) \otimes A_{1g,2u} &= A_{1u}(0) + A_{2u}(0) + A_{1g}(0) + A_{2u}(0) \\ &+ (B'(k') + B'(-k')) + (B''(k') + B''(-k')) + E_{\tilde{\mu}'g}(0) + E_{\tilde{\mu}'u}(0) + (E_{n-\tilde{\mu}'}(k') + E_{n-\tilde{\mu}'}(-k')).\end{aligned} \tag{58}$$

Note that the same decomposition of symmetries is found for even (A_{1g}) and odd (A_{2u}) envelope functions. The excitons with band edges at the center of the Brillouin zone ($K=0$) are obtained from the product between the electron and hole states with opposite wavevectors ($k_e=-k_h=\pm k_0$), while the band edge states at $K=k'$ are obtained from electrons and holes with equal wavevectors $k_e=k_h=\pm k_0$. It is important to mention that the direct product between $E_{\tilde{\mu}}$ states will always lead to A and E symmetry states. However, since $k_0 \sim 2\pi/3a$, then $2k_0$ always crosses the boundary of the first Brillouin zone, and therefore the A and E symmetry states obtained from the direct product need to be translated back into the first Brillouin zone by the procedure described in Section 2.4.2 and explicitly applied to the (6, 5) nanotube in Section 8.1.1. The A' and A'' states obtained from the direct product will have their parities exchanged and thus lead to B' and B'' states while the $E_{\tilde{\mu}'}$ states will have their quasi-angular quantum number $\tilde{\mu}'$ corrected to $n-\tilde{\mu}'$, as indicated in Eq. (58). In Fig. 18(f) we show a schematic diagram for the 16exciton states obtained for $v=0$ in armchair SWNTs.

For E_{ij} transitions with $i \neq j$ and quasi-angular momentum differing by ± 1, we have

$$\begin{aligned}&(E_{\tilde{\mu}}(k_0)+E_{\tilde{\mu}\pm1}(-k_0)) \otimes \left(E_{\tilde{\mu}}(k_0)+E_{\tilde{\mu}\pm1}(-k_0)\right) \otimes A_{1g,2u} \\ &\quad = E_{1g}(0)+E_{1u}(0)+E_{\tilde{\mu}'g}(0)+E_{\tilde{\mu}'u}(0)+2E_{n-1}(\pm k')+2E_{n-\tilde{\mu}'}(\pm k'),\end{aligned} \tag{59}$$

for both A_{1g} and A_{2u} envelope functions.

8.2. Selection rules for optical absorption

To obtain the selection rules for the optical absorption of the excitonic states, it is necessary to consider that the ground state of the nanotube transforms as a totally symmetric representation (A_1 for chiral and A_{1g} for achiral nanotubes) and that only $K=0$ excitons can be created due to linear momentum conservation. For light polarized parallel to the nanotube axis the interaction between the electric field and the electric dipole in the nanotube transforms as the A_2 (A_{2u}) representation for chiral (achiral) nanotubes. Thus, one photon excitation will create A_2 (A_{2u}) excitonic states. The same is true for the emission of a photon by excitonic recombination.

Since only A_2 (A_{2u}) symmetry excitons are optically active for parallel polarized light, only one of the 4 excitons obtained for each envelope function v and associated with an E_{ii} transition is optically active, the remaining three being dark states. The same applies for the 16 exciton states in armchair tubes, described by Eq. (58). However, for zigzag tubes, one can see from Eq. (54) and Eq. (55) that only states with v even (envelope functions even under $z \to -z$) will have a bright exciton. The differences in the symmetry properties of chiral, zigzag and armchair nanotubes need to be taken into account when using specific nanotubes as representatives of optical properties occurring generally for carbon nanotubes.

It is interesting to comment on the existence of a bright exciton for odd v states in chiral and armchair tubes. From an analogy to the simple 1D hydrogen atom, one would expect odd envelope functions to give rise to dark states. However, an even wavefunction can also be constructed by the product of an odd Bloch function and an odd envelope function. Nevertheless, although being formally bright, we expect a very low oscillation strength for these excitons, since an odd envelope function should give a very low probability of finding electron and hole at the same position for recombination. Therefore, it is clear that the experimental Kataura plot, though initially constructed for band-band transitions [52,53], will nevertheless give a very similar picture when constructed for excitons. Although the excitonic picture is more complex, having up to 16 excitonic ground states for each band-band transition, plus excited excitonic states, most of the excitonic states are dark (not active optically) or have a very weak oscillator strength. The Kataura plot can, therefore, be interpreted as a plot of the energy of the bright exciton state with $v=0$ as a function of tube diameter.

However, odd v states are also important for the interpretation of the two-photon absorption experiments performed to prove the excitonic nature of the optical transition in carbon nanotubes [36,37]. In 2-photon excitation experiments, the incident photons should create A_1 (A_{1g}) symmetry excitons, since $A_2 \otimes A_2 = A_1$ (or $A_{2u} \otimes A_{2u} = A_{1g}$ for achiral tubes). Therefore, for zigzag tubes (see Eq. (55)), only the states with odd envelope functions will be accessible by two-photon transitions. For chiral (armchair) tubes, in principle all values of v should contain an A_1 (A_{1g}) symmetry exciton [54].

For light polarized perpendicular to the nanotube axis, the electron–photon interaction transforms as one of the $\mathbb{E}_{\pm1}$ (E_{1u}) representations. Thus, only excitonic states with $E_{\pm1}$ (E_{1u}) symmetries can be accessed using perpendicularly polarized light. As described in Eqs. (54) and (59), such excitons are present for every value of v in chiral and armchair

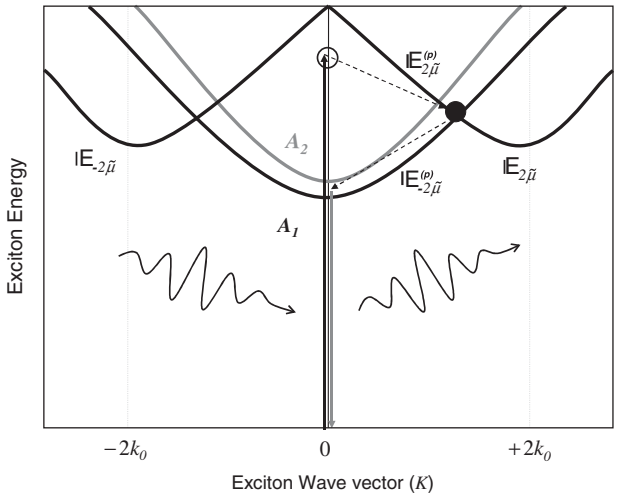

Fig. 19. Diagram showing a possible double resonance process. The A_2 symmetry exciton is created by 1-photon absorption. This exciton is scattered to a state with $\mathbb{E}_{2\tilde{\mu}}$ symmetry by a $\mathbb{E}_{2\tilde{\mu}}$ symmetry phonon, and then scattered back to $K = 0$ by another phonon with $\mathbb{E}_{-2\tilde{\mu}}$ symmetry. The last step can take the exciton either to states with A_1 or A_2 symmetries.

tubes as long as sub-bands of adjacent indices, namely $\tilde{\mu}$ and $\tilde{\mu} \pm 1$, are coupled. Once again the selection rules for zigzag tubes are more restrictive: Only states with even v and coupling bands of opposite parity or odd v and coupling bands of the same parity are bright under perpendicular polarization. However, with the exception of zigzag nanotubes, the excitons which are active for perpendicular polarized light have a band edge at a wavevector $k' \neq 0$, and therefore, its optical excitation is, in principle, forbidden by the conservation of linear momenta.

8.3. Selection rules for Raman scattering processes

The selection rules for first-order Raman scattering will not, as a first approximation, be affected by the excitonic interaction. The main effect of excitonic states in Raman spectroscopy is the fact that only the A_2 (A_{2u}) symmetry excitons can resonantly absorb or emit photons.

The double resonance process involves a transition between different exciton states assisted by a phonon. Thus, it is possible to use symmetry-based selection rules to determine the allowed transitions for a given phonon. To illustrate this, we show in Fig. 19 a possible double resonance process for a chiral nanotube. Here, the first optical transition occurs by the creation of an A_2 symmetry exciton, which is off-resonance, as indicated in Fig. 19, and therefore A_2 in this case is a virtual state. This virtual excitonic state is then scattered by a phonon with $\mathbb{E}^{(p)}_{2\tilde{\mu}}$ symmetry, where (p) stands for phonon, to an excitonic state with $\mathbb{E}_{2\tilde{\mu}}$ symmetry. This $\mathbb{E}_{2\tilde{\mu}}$ exciton, can then be scattered back to an A symmetry exciton by another phonon with $\mathbb{E}^{(p)}_{-2\tilde{\mu}}$ symmetry. As explained in Section 8.1.1, there are two exciton bands with A symmetry for each envelope function v, one which has A_1 symmetry at $K = 0$ and another which, at $K = 0$, has A_2 symmetry. The energy difference between these two states is expected to be a few meV [46,47,55,56], and therefore the double resonance process should create excitons in both states with approximately equal probability. However, this energy difference depends on $1/d_t^2$ [57] and can play an important role for smaller diameter nanotubes.

Noted that, as explained in Section 8.1.1, the $E_{2\tilde{\mu}}$ exciton state discussed here is formed from the combination of the VHSs in the electronic bands associated with index $\tilde{\mu}$. Therefore, this double resonance process is equivalent to the process discussed in Section 7.3 within the single particle approximation. It can be seen that, from the standpoint of group theory, the double resonance process within the excitonic picture is similar to that for one-electron bands since it gives the same quantum numbers for the phonon which couples the given states. However, for excitons formed through the mixing of $\mathbb{E}_{\tilde{\mu}}$ and $\mathbb{E}_{-\tilde{\mu}}$ symmetry electronic bands, the resulting $\mathbb{E}_{\pm 2\tilde{\mu}}$ symmetry excitons have different energies from that of A symmetry excitons. This energy difference can either enhance or quench the double resonance process for a specific phonon depending on whether the intermediate state of the double resonance process comes closer to the $\mathbb{E}_{\pm 2\tilde{\mu}}$ symmetry band edge, or farther from it. Thus, it is very important to take into consideration the energy

splitting between the A and E symmetry excitons for evaluating the frequency and intensity of double resonance Raman peaks. Calculations of the excitonic binding energies have found a splitting between the A and E symmetry excitons ranging from 5 to 15 meV [46,47,55,56]. This energy difference will only affect double resonance processes for which one of the phonons involved in the process is an acoustic mode [58,59]. However, it is clear that by mixing different electronic bands, it is possible to create different excitons with very different symmetries and energies. Although optical transitions for these excitons will all be forbidden, they can be accessed through exciton–phonon coupling and other symmetry breaking interactions, and thus can contribute to double resonance processes. In fact, the Raman spectra of carbon nanotubes are populated with Raman peaks which cannot be directly associated with Γ point phonons, such as the D-band, G′-band, the intermediate frequency modes [58,59], and other combination modes [60]. A more accurate description of the processes giving rise to these Raman modes will have to take into account the excitonic nature of the optical transitions. However, to obtain the energy of these mixed excitons, and thus to calculate the resonance condition for these double resonance processes, it is necessary to solve the Bethe–Salpeter equation considering all the possible values of k and $\tilde{\mu}$ labeling the electron and hole eigenfunctions.

9. Summary and conclusions

In this work we have reviewed the space group theory of carbon nanotubes giving a detailed summary of the symmetry operations exhibited by chiral and achiral nanotubes, as well as finding the irreducible representations within the formalism of factor groups. The irreducible representations of the groups of the wavevector of nanotubes were directly obtained and the quantum numbers were associated with linear and helical momenta. The electronic and vibrational properties of carbon nanotubes were discussed from the standpoint of group theory. We also discussed the symmetry properties of carbon nanotubes from the "zone-folding" standpoint, resulting from the presence of compound operations. The compound operations allow the geometrical construction of the nanotube as a 2D structure from a 2-atom unit cell, which can be directly compared to the graphene layer. In this sense, most of the symmetry properties of carbon nanotubes can be understood as momentum conservation laws for the 2D nanotube structure.

A comparison between the formalism of line groups and that of the factor group of the wavevector, which is commonly used for obtaining the irreducible representations of space groups, is performed in this review article to provide a bridge between the different analysis which have been used in the literature of SWNTs. The irreducible representations of the line groups are compared to those of the group of the wavevector, and the quantum numbers are associated with a helical momentum and a pure angular momentum. For completeness, we obtained the symmetry properties of electronic states of chiral nanotubes using the line group approach and compared them directly with the symmetries of the electronic states obtained from the formalism of the group of the wavevector. It was noted that a direct comparison could only be made for specific points of the nanotube 1D Brillouin zone. This limitation can be attributed to the 2D nature of the helical momentum, and can be overcome by using the "zone-folding" scheme to relate the two formalisms.

The symmetries of the electron and phonon eigenstates and the selection rules for electron–photon and electron–phonon interactions were used to give insight into the dynamics of optical processes which are commonly used in the study of carbon nanotubes, such as optical absorption and Raman scattering processes. These properties were first analyzed neglecting the excitonic nature of the optical transitions. However, in view of the fact that the electron–electron and electron–hole interactions are significantly enhanced in a 1D system, we included a brief discussion of excitonic effects in SWNTs and obtained the exciton symmetries using a simple model for the electron–hole interaction. It is interesting to note that the symmetry properties of excitons in carbon nanotubes are different from those of excitons in typical semiconductors and organic conductors due to the presence of two degenerate states contributing to their formation. The selection rules for the optical absorption and Raman scattering, including double resonance processes, are discussed in terms of the excitonic symmetries.

Acknowledgments

The authors would like to Acknowledge Dr. R. Saito for his careful reading of the manuscript and very helpful discussions. The MIT authors acknowledge support under NSF Grant DMR04-05538. Authors E. B. B. and A. G. S. F. acknowledge financial support from FUNCAP-Brasil and CAPES-Brasil (PRODOC). Authors A. J. and R. B. C. acknowledge support from CNPq, Brasil and Faperj, respectively. Brazilian authors acknowledge support from Instituto de Nanotecnologia and Rede Nacional de Pesquisa em Nanotubos de Carbono.

References

[1] R.A. Jishi, D. Inomata, K. Nakao, M.S. Dresselhaus, G. Dresselhaus, J. Phys. Soc. Jpn. 63 (1994) 2252.
[2] M.S. Dresselhaus, R.A. Jishi, G. Dresselhaus, D. Inomata, K. Nakao, R. Saito, Mol. Mater. 4 (1994) 27.
[3] R. Saito, G. Dresselhaus, M.S. Dresselhaus, Physical Properties of Carbon Nanotubes, Imperial College Press, London, 1998.
[4] M. Damnjanović, I. Milosević, T. Vuković, R. Sredanović, Phys. Rev. B 60 (1999) 2728.
[5] M. Damnjanović, T. Vuković, I. Milosević, J. Phys. A: Math. Gen. 33 (2000) 6561.
[6] O.E. Alon, Phys. Rev. B 63 (2001) 201403(R).
[7] O.E. Alon, J. Phys.: Condens. Matter 15 (2003) 2489.
[8] M.S. Dresselhaus, G. Dresselhaus, A. Jorio, Applications of Group Theory to the Physics of Condensed Matter, Springer, New York, 2006.
[9] G.G. Samsonidze, A. Grüneis, R. Saito, A. Jorio, A.G. Souza Filho, G. Dresselhaus, M.S. Dresselhaus, Phys. Rev. B 69 (2004) 205402.
[10] Z.K. Tang, H.D. Sun, J. Wang, J. Chen, G. Li, Appl. Phys. Lett. 73 (1998) 2287.
[11] V.N. Popov, N. J. Phys. 6 (2004) 17.
[12] G.G. Samsonidze, R. Saito, N. Kobayashi, A. Grüneis, J. Jiang, A. Jorio, S.G. Chou, G. Dresselhaus, M.S. Dresselhaus, Appl. Phys. Lett. 85 (2004) 5703.
[13] C.T. White, D.H. Robertson, J.W. Mintmire, Phys. Rev. B 47 (1993) 5485.
[14] G.G. Samsonidze, R. Saito, A. Jorio, M.A. Pimenta, A.G. Souza Filho, A. Grüneis, G. Dresselhaus, M.S. Dresselhaus, J. Nanosci. Nanotechnol. 3 (2003) 431.
[15] The general concept of weak-direct product is defined on the following way: A Group G is said to be the weak-direct product of its subgroups H and K when (i) the identity element is the only intersection of H and K and (ii) each element of G is the product of one element in H with one element in K. Semi-direct and direct products are special cases of weak-direct products. When H and K are invariant subgroups, the result is a direct product. When only H is an invariant subgroup, the result is a semi-direct product.
[16] J.F. Cornwell, Group theory and electronic energy bands in solids, Series of Monographs on Selected Topics in Solid State Physics, Wiley, New York, 1969.
[17] Two integers are coprime if they share no common positive factors (divisors) except 1.
[18] A sub-group $\mathfrak{T}$ of G is said to be invariant, or self-conjugate, if $g^{-1}\mathfrak{T}g$ is identical with $\mathfrak{T}$ for all elements g of G.
[19] The rod group can be obtained by considering the operations of the space group formed by the space group operations, setting all translations (pure and compound) to zero. The rod group is isomorphic to the group of the wavevector $k = 0$.
[20] M. Vujičić, I.B. Božović, F. Herbut, J. Phys. A: Math. Gen. 10 (1977) 1271.
[21] M. Damnjanović, M. Vujičić, Phys. Rev. B 25 (1982) 6987.
[22] I.B. Božović, M. Vujičić, F. Herbut, J. Phys. A: Math. Gen. 11 (1978) 2133.
[23] I.B. Božović, M. Vujičić, J. Phys. A: Math. Gen. 14 (1981) 777.
[24] M. Damnjanović, I. Milosević, T. Vuković, J. Maultzsch, J. Phys. A 36 (2003) 5707.
[25] T. Vuković, I. Milošević, M. Damnjanović, Phys. Rev. B 65 (2002) 045418.
[26] C. Zhou, J. Kong, H. Dai, Phys. Rev. Lett. 84 (2000) 5604.
[27] R.A. Jishi, S. Inomata, K. Nakao, M.S. Dresselhaus, G. Dresselhaus, J. Phys. Soc. Jpn. B 63 (1994) 2252.
[28] A. Kleiner, S. Eggert, Phys. Rev. B 63 (2001) 073408.
[29] R. Saito, K. Sato, Y. Oyama, J. Jiang, G.G. Samsonidze, G. Dresselhaus, M.S. Dresselhaus, Phys. Rev. B 71 (2005) 153413.
[30] A. Jorio, C. Fantini, M.A. Pimenta, R.B. Capaz, G.G. Samsonidze, G. Dresselhaus, M.S. Dresselhaus, J. Jiang, N. Kobayashi, A. Grüneis, R. Saito, Phys. Rev. B 71 (2005) 075401.
[31] R. Saito, G. Dresselhaus, M.S. Dresselhaus, Physical Properties of Carbon Nanotubes, 1st ed., Imperial College Press, London, 1998.
[32] O. Dubay, G. Kresse, Phys. Rev. B 67 (2003) 035401 ⟨http://link.aps.org/abstract/PRB/v67/e035401⟩.
[33] K.-P. Bohnen, R. Heid, H.J. Liu, C. Chan, Phys. Rev. Lett. 93, 24551 (Lattice Dynamics and Electron–Phonon Interaction in (3, 3) Carbon Nanotubes).
[34] L. Wirtz, A. Rubio, Solid State Commun. 131 (2004) 141.
[35] T. Ando, J. Phys. Soc. Jpn. 66 (1997) 1066.
[36] F. Wang, G. Dukovic, L.E. Brus, T.F. Heinz, Science 308 (2005) 838.
[37] J. Maultzsch, R. Pomraenke, S. Reich, E. Chang, D. Prezzi, A. Ruini, E. Molinari, M.S. Strano, C. Thomsen, C. Lienau, Phys. Rev. B 72 (2005) 241402(R).
[38] R.M. Martin, L.M. Falicov, Light Scattering in Solids, Springer, Berlin, 1975 p. 80.
[39] M. Cardona, Light Scattering in Solids, Springer, Berlin, 1982.
[40] A. Jorio, M.A. Pimenta, A.G. Souza Filho, G.G. Samsonidze, A.K. Swan, M.S. Ünlü, B.B. Goldberg, R. Saito, G. Dresselhaus, M.S. Dresselhaus, Phys. Rev. Lett. 90 (2003) 107403.
[41] A. Jorio, A.G. Souza Filho, V.W. Brar, A.K. Swan, M.S. Ünlü, B.B. Goldberg, A. Righi, J.H. Hafner, C.M. Lieber, R. Saito, et al., Phys. Rev. B 65 (2002) 121402.
[42] C. Thomsen, S. Reich, Phys. Rev. Lett. 85 (2000) 5214.
[43] R. Saito, A. Grüneis, G.G. Samsonidze, V.W. Brar, G. Dresselhaus, M.S. Dresselhaus, A. Jorio, L.G. Cançado, C. Fantini, M.A. Pimenta, A.G. Souza Filho, N. J. Phys. 5 (2003) 157.1.
[44] R. Saito, G. Dresselhaus, M.S. Dresselhaus, Phys. Rev. B 61 (2000) 2981.
[45] A. Grüneis, R. Saito, G.G. Samsonidze, T. Kimura, M.A. Pimenta, A. Jorio, A.G.S. Filho, G. Dresselhaus, M.S. Dresselhaus, Phys. Rev. B 67 (2003) 165402.
[46] V. Perebeinos, J. Tersoff, P. Avouris, Phys. Rev. Lett. 94 (2005) 027402.

[47] C.D. Spataru, S. Ismail-Beigi, L.X. Benedict, S.G. Louie, Phys. Rev. Lett. 92 (2004) 077402.
[48] M.S. Dresselhaus, G. Dresselhaus, R. Saito, A. Jorio, Exciton Photophysics of Carbon Nanotubes, Annual Reviews of Physical Chemistry Chemical Physics 58, Intelligent Synthesis of the Scientific Literature, Palo Alto, 2007 (to be published).
[49] M. Rohlfing, S.G. Louie, Phys. Rev. B 62 (2000) 4927.
[50] R.S. Knox, Theory of Excitons, vol. 5 (Suppl.) Solid State Physics, Academic Press, New York, 1963.
[51] R. Loudon, Am. J. Phys. 27 (1959) 649.
[52] S.M. Bachilo, M.S. Strano, C. Kittrell, R.H. Hauge, R.E. Smalley, R.B. Weisman, Science 298 (2002) 2361.
[53] R.B. Weisman, S.M. Bachilo, Nanoletters 3 (2003) 1235.
[54] E.B. Barros, G.G. Samsonidze, A.G. Souza Filho, A. Jorio, C.D. Spataru, S. Ismail-Beigi, R.B. Capaz, S.G. Louie, G. Dresselhaus, M.S. Dresselhaus, Phys. Rev. B 73 (2006) 241406(R).
[55] C.D. Spataru, S. Ismail-Beigi, L.X. Benedict, S.G. Louie, Appl. Phys. A 78 (2004) 1129.
[56] C.D. Spataru, S. Ismail-Beigi, R.B. Capaz, S.G. Louie, Phys. Rev. Lett. 95 (2004) 247402.
[57] R.B. Capaz, C.D. Spataru, S. Ismail-Beigi, S.G. Louie, cond-mat/0606474.
[58] C. Fantini, A. Jorio, M. Souza, L.O. Ladeira, M.A. Pimenta, A.G. Souza Filho, R. Saito, G.G. Samsonidze, G. Dresselhaus, M.S. Dresselhaus, Phys. Rev. Lett. 93 (2004) 087401.
[59] C. Fantini, A. Jorio, M. Souza, R. Saito, G.G. Samsonidze, M.S. Dresselhaus, M.A. Pimenta, Phys. Rev. B 72 (2005) 085446.
[60] V.W. Brar, G.G. Samsonidze, G. Dresselhaus, M.S. Dresselhaus, R. Saito, A.K. Swan, M.S. Ünlü, B.B. Goldberg, A.G. Souza Filho, A. Jorio, Phys. Rev. B 66 (2002) 155418.